This is a preprint, the final version is subject to change, of the American Mineralogist (MSA)
Cite as Authors (Year) Title. American Mineralogist, in press.
(DOI will not work until issue is live.) DOI: http://dx.doi.org/10.2138/am-2017-5823

Revision 1

Revisiting the electron microprobe method of spinel-olivine-orthopyroxene oxybarometry applied to spinel peridotites

Fred A Davis*[1,2], Elizabeth Cottrell[1], Suzanne K Birner[1,3], Jessica M Warren[4], Oscar G Lopez[1]

[1]National Museum of Natural History, Smithsonian Institution, Washington, DC 20560, USA

[2]Department of Earth and Environmental Sciences, University of Minnesota Duluth, Duluth, MN 55812, USA

[3]Department of Geological Sciences, Stanford University, Stanford, CA 94305, USA

[4]Department of Geological Sciences, University of Delaware, Newark, DE 19716, USA

*corresponding author, email: fdavis@d.umn.edu; tel: 1-218-726-8331

Abstract

Natural peridotite samples containing olivine, orthopyroxene, and spinel can be used to assess the oxygen fugacity (f_{O2}) of the upper mantle. The method requires accurate and precise quantification of spinel $Fe^{3+}/\Sigma Fe$ ratios. Wood and Virgo (1989, *Geochim. Cosmochim. Acta*) presented a correction procedure for electron microprobe (EPMA) measurements of spinel $Fe^{3+}/\Sigma Fe$ ratios that relies on a reported correlation between the difference in $Fe^{3+}/\Sigma Fe$ ratio by Mössbauer spectroscopy and by electron microprobe ($\Delta Fe^{3+}/\Sigma Fe^{Möss\text{-}EPMA}$) and the Cr# (Cr/(Al+Cr)) of spinel. This procedure has not been universally adopted, in part, because of debate as to the necessity and effectiveness of the correction. We have performed a series of replicate EPMA analyses of several spinels, previously characterized by Mössbauer spectroscopy, to test the accuracy and precision of the Wood and Virgo correction. While we do not consistently observe a correlation between Cr# and $\Delta Fe^{3+}/\Sigma Fe^{Möss\text{-}EPMA}$ in measurements of the correction standards, we nonetheless find that accuracy of $Fe^{3+}/\Sigma Fe$ ratios determined for spinel samples treated as unknowns improves when the correction is applied. Uncorrected measurements have a mean $\Delta Fe^{3+}/\Sigma Fe^{Möss\text{-}EPMA} = 0.031$ and corrected measurements have a mean $\Delta Fe^{3+}/\Sigma Fe^{Möss\text{-}EPMA} = -0.004$. We explain how the reliance of the correction on a global correlation between Cr# and MgO concentration in peridotitic spinels improves the accuracy of $Fe^{3+}/\Sigma Fe$ ratios despite the absence of a correlation between $\Delta Fe^{3+}/\Sigma Fe^{Möss\text{-}EPMA}$ and Cr# in some analytical sessions.

Precision of corrected $Fe^{3+}/\Sigma Fe$ ratios is dependent on the total concentration of Fe, and varies from ±0.012 to ±0.032 (1σ) in the samples analyzed; precision of uncorrected analyses is poorer by approximately a factor of two. We also present an examination of the uncertainties in the calculation contributed by the other variables used to derive f_{O2}. Because there is a logarithmic relationship between the activity of magnetite and $\log f_{O2}$, the uncertainty in f_{O2} relative to the

QFM buffer contributed by the electron microprobe analysis of spinel is asymmetrical and larger at low ferric Fe concentrations ($^{+0.3}_{-0.4}$ log units, 1σ, at $Fe^{3+}/\Sigma Fe = 0.10$) than at higher ferric Fe concentrations (±0.1 log units, 1σ, at $Fe^{3+}/\Sigma Fe = 0.40$). Electron microprobe analysis of olivine and orthopyroxene together contribute another ±0.1 to ±0.2 log units of uncertainty (1σ). Uncertainty in the temperature and pressure of equilibration introduce additional errors on the order of tenths of log units to the calculation of relative f_{O2}. We also document and correct errors that appear in the literature when formulating f_{O2} that, combined, could yield errors in absolute f_{O2} of greater than 0.75 log units – even with perfectly accurate $Fe^{3+}/\Sigma Fe$ ratios. Finally, we propose a strategy for calculating the activity of magnetite in spinel that preserves information gained during analysis about the ferric iron content of the spinel. This study demonstrates the superior accuracy and precision of corrected EPMA measurements of spinel $Fe^{3+}/\Sigma Fe$ ratios compared to uncorrected measurements. It also provides an objective method for quantifying uncertainties in the calculation of f_{O2} from spinel peridotite mineral compositions.

Keywords:
Mössbauer Spectroscopy; Oxygen Fugacity; Electron Microprobe; Oxybarometry; Xenolith

Introduction

Estimates of mantle oxygen fugacity (f_{O2}) are necessary to predict stable phase assemblages in the mantle, particularly C and S bearing phases. Records of mantle f_{O2} include mineral oxybarometers (e.g., Buddington and Lindsley 1964; O'Neill and Wall 1987; Gudmundsson and Wood 1995), $Fe^{3+}/\Sigma Fe$ ratios of basaltic glasses (e.g., Christie et al. 1986; Bézos and Humler 2005; Cottrell et al. 2009), and abundances and ratios of redox-sensitive trace elements in basalts and peridotites (e.g., Shervais 1982; Canil 1999; Li and Lee 2004). Mineral oxybarometers that can be applied to peridotite samples provide direct estimates of f_{O2} in the upper mantle and play a key role in deciphering past and present mantle f_{O2} conditions.

We can determine upper mantle f_{O2} directly from peridotites containing the assemblage olivine+orthopyroxene+spinel if we know or assume the pressure-temperature conditions following the reaction:

$$\underset{olivine}{6Fe_2SiO_4} + O_2 \leftrightarrow \underset{opx}{3Fe_2Si_2O_6} + \underset{spinel}{2Fe_3O_4} \quad (1)$$

Several studies have parameterized f_{O2} based on this equilibrium (O'Neill and Wall 1987; Mattioli and Wood 1988; Wood 1991), and Wood (1990) tested this equilibrium experimentally. An accurate measurement of the oxidation state of Fe in the spinel phase is required to apply these parameterizations. The ratio of ferric iron to total iron ($Fe^{3+}/\Sigma Fe = Fe^{3+}/[Fe^{3+} + Fe^{2+}]$) in spinel can be measured by Mössbauer spectroscopy (e.g., Wood and Virgo 1989); however, traditional Mössbauer analysis is restricted to large volumes of sample. Removing spinel from its host rock for bulk Mössbauer analysis is labor intensive, can lead to averaging of spinels that are chemically heterogeneous on the hand-sample scale, and may lead to contamination of the Mössbauer spectra by other phases (Wood and Virgo 1989; Ballhaus et al. 1991; Woodland et al.

1992). In addition, Mössbauer analysis requires equipment that is expensive to run and expertise that may not be readily available. Thus, Wood and Virgo (1989) developed the electron probe microanalysis (EPMA) technique for determining $Fe^{3+}/\Sigma Fe$ ratios in spinel by in situ analysis.

Spinel $Fe^{3+}/\Sigma Fe$ ratios can be determined from an EPMA measurement by assuming ideal stoichiometry of the spinel phase and assigning cations of Fe as ferric in a proportion that balances the negative charge that arises from the initial assumption that all the iron is ferrous (Stormer 1983). This method can lead to large uncertainties on calculated $Fe^{3+}/\Sigma Fe$ ratios because the analytical errors for each oxide propagate through the calculation (e.g., Dyar et al. 1989; Wood and Virgo 1989). Wood and Virgo (1989) lessened this uncertainty by correcting their analyses using a set of spinel standards with $Fe^{3+}/\Sigma Fe$ ratios that they determined by Mössbauer spectroscopy. Their correction, hereafter referred to as "W&V89" used a reported correlation between the difference in $Fe^{3+}/\Sigma Fe$ ratio by Mössbauer and by EPMA ($\Delta Fe^{3+}/\Sigma Fe^{Möss-EPMA}$) and the Cr# (Cr/[Al+Cr]) of the spinels.

Subsequent studies of spinel peridotite oxybarometry have disagreed over the value and effectiveness of the W&V89 correction. The W&V89 correction has been applied as originally described in many studies (e.g., Woodland et al. 1992; Parkinson and Pearce 1998; Dare et al. 2009). Others have challenged the premise of the correction or modified its application. Ballhaus et al. (1991) questioned the need to apply any correction to $Fe^{3+}/\Sigma Fe$ ratios measured by EPMA, noting in particular a close agreement between $\log f_{O2}$ calculated from both EPMA and Mössbauer analyses of the same spinel samples. Luhr and Aranda-Gomez (1997) required a correction to their spinel analyses to reproduce the Mössbauer $Fe^{3+}/\Sigma Fe$ ratios of their spinel standards, but did not observe the correlation between $\Delta Fe^{3+}/\Sigma Fe^{Möss-EPMA}$ and the Cr# described by Wood and Virgo (1989). They chose to apply a single, constant-offset correction to their

spinel $Fe^{3+}/\Sigma Fe$ ratios rather than apply the W&V89 correction in the absence of an underlying correlation.

Below we demonstrate that the W&V89 correction substantially improves both accuracy and precision of spinel $Fe^{3+}/\Sigma Fe$ ratios determined by EPMA. Biases in uncorrected EPMA determinations of $Fe^{3+}/\Sigma Fe$ ratios do not result from any inherent bias in the EPMA analysis or the applied matrix corrections, but instead result from session-to-session variations in analyses of primary standards. We present replicate analyses by EPMA of several spinels previously characterized by Mössbauer spectroscopy, which demonstrate the effectiveness of the W&V89 correction and elucidate the underlying mechanisms that drive the W&V89 correction. In particular, we focus on the relationship between $\Delta Fe^{3+}/\Sigma Fe^{\text{Möss-EPMA}}$ and Cr# described by Wood and Virgo (1989) and how the W&V89 correction functions when this correlation is weak or absent. We also demonstrate that a global correlation between Cr# and MgO concentration in natural peridotite-hosted spinels allows the W&V89 correction to improve accuracy and precision of $Fe^{3+}/\Sigma Fe$ ratios, even when elements other than Al and Cr are responsible for the analytical bias.

Our replicate analyses of Mössbauer-characterized spinels allow us to estimate the precision of $Fe^{3+}/\Sigma Fe$ ratios determined by EPMA and corrected following the W&V89 method. We also discuss the propagation of uncertainties in the measurements of spinel, olivine, and orthopyroxene and in the estimates of pressure and temperature of equilibration through the f_{O2} calculation. We present new analyses of several spinel peridotites from Hawaii to demonstrate the effect of precision in the analysis of spinel $Fe^{3+}/\Sigma Fe$ concentration on calculated f_{O2}. We present analyses of spinels from a peridotite from Tonga to demonstrate the diminished precision

of the $Fe^{3+}/\Sigma Fe$ measurement of unknown spinels with compositions that depart from the Cr#-MgO trend of the correction standards.

Samples and Methods

Samples Analyzed

We analyzed 32 spinel samples, kindly provided by B. Wood, for major and minor elements by electron microprobe with the goal of determining $Fe^{3+}/\Sigma Fe$ ratios. These spinels, which we refer to collectively as the "Wood spinels", were previously examined by Wood and Virgo (1989), Bryndzia and Wood (1990), and Ionov and Wood (1992). Each has been previously analyzed by Mössbauer spectroscopy, which provides an independent estimate of the $Fe^{3+}/\Sigma Fe$ ratio. The Wood spinels are separates from peridotites representing a diversity of major element compositions (Cr# = 0.04-0.57), Fe oxidation states (Mössbauer $Fe^{3+}/\Sigma Fe$ = 0.058-0.32), and geological environments (continental and arc peridotite xenoliths, abyssal peridotites).

Four spinel peridotite samples from Hawaii were analyzed in order to test the individual contributions of each mineral phase (e.g,. olivine and orthopyroxene in addition to spinel) to the total uncertainty in the f_{O2} calculation. The Hawaiian samples are spinel lherzolite xenoliths from Salt Lake Crater, Oahu, originally collected by E. Dale Jackson and now part of the National Rock and Ore Collection at the Smithsonian Institution National Museum of Natural History. We also analyzed spinels from a harzburgite (BMRG08-98-2-2) dredged from the Tonga trench during the 1996 Boomerang cruise (Bloomer et al. 1996; Wright et al. 2000); the spinel in this sample has Cr# and MgO concentrations that depart significantly from the trend of the spinels used to correct $Fe^{3+}/\Sigma Fe$ ratios.

Analytical methods

We analyzed spinel, olivine, and orthopyroxene at the Smithsonian Institution using a JEOL 8900 Superprobe with 5 wavelength dispersive spectrometers (WDS). Table 1 provides information on our primary standards, count times, and detector crystals, and additional information about the electron microprobe analyses is given in the Supplementary Material.

We analyzed spinels in two different types of analytical sessions. First, we analyzed the 32 Wood spinels without correcting $Fe^{3+}/\Sigma Fe$ ratios (sessions S1-S3, Table 2 and Supplementary Table S1) to determine the range of compositions present, to reveal compositional systematics, and to check for intra- and intergranular heterogeneity of the samples. Out of the 32 Wood spinels, we chose 7 as correction standards (hereafter, the correction set; selection criteria given in Results). The correction set spinels are the standards that we use to determine the $Fe^{3+}/\Sigma Fe$ correction to be applied to a given analytical session. In this second type of analytical session the correction set was analyzed along with another subset of the Wood spinels treated as unknowns (hereafter, the validation set) and the Tongan and Hawaiian spinels (Sessions A1-A4 and B1-B4, Supplementary Table S2).

In sessions S1-S3, we analyzed one to six individual grains of each of the Wood spinels. From each grain, we analyzed three to ten points, depending upon the total number of grains analyzed (Supplementary Table S1), except for the samples made from crushed Mössbauer powders. We collected only one analytical point on each grain of these powdered samples. We analyzed secondary standards of chromite, Cr-augite, and hypersthene (Jarosewich et al. 1980, 1987) every two to four hours during the session to monitor instrumental drift.

In sessions A1-A4 and B1-B4, we collected three analytical points on each sample in the correction set both before and after analyzing unknowns, corresponding to re-analysis of the correction standards after 12-14 hours. We analyzed secondary standards at regular intervals as described above. In these sessions, individual analyses were discarded when totals fell outside the range 97%-101%; this range is asymmetrical around 100% because we expect samples with high Fe^{3+} to give relatively low totals when total Fe is calculated as FeO. We also excluded individual analyses that contained $SiO_2 > 0.3$ wt.% to avoid analyses that may have sampled surrounding silicate material. To ensure that each session could be considered separately in terms of intersession reproducibility, the filament was turned down and allowed to cool for at least 12 hours and then saturated again at the start of each new session, even when these sessions occurred on consecutive days.

We analyzed the major-element compositions of olivine and orthopyroxene from the four Hawaiian xenoliths in a single analytical session by analyzing the core compositions of 10 different grains of each mineral in each sample (Table 3).

The spinel $Fe^{3+}/\Sigma Fe$ ratio correction method

We applied the W&V89 correction to spinels analyzed in sessions A1-A4 and B1-B4. We calculated $Fe^{3+}/\Sigma Fe$ ratio and Cr# of each of the correction set spinels measured both at the beginning and end of the analytical session. We calculated the $Fe^{3+}/\Sigma Fe$ ratios of the spinels by normalizing the spinel cation proportions to 3 total cations, treating all Fe as Fe^{2+}, and then adjusting the Fe^{3+}/Fe^{2+} ratio to balance the charge deficiency or excess (Stormer 1983). Occasionally, spinels with low $Fe^{3+}/\Sigma Fe$ ratios gave a small positive charge excess, which was balanced by allowing negative contributions to Fe^{3+}.

We calculated $\Delta Fe^{3+}/\Sigma Fe^{\text{Möss-EPMA}}$ for each measurement and determined the best fit line through all measurements of the correction set to determine slope and intercept (Wood and Virgo 1989):

$$\Delta Fe^{3+}/\Sigma Fe^{Möss\text{-}EPMA} = A*Cr\# + B \quad (2)$$

We used the resulting slope and intercept to correct the calculated $Fe^{3+}/\Sigma Fe$ ratios of all other spinels measured during that session. To maintain consistency in data processing, we applied this correction irrespective of whether $\Delta Fe^{3+}/\Sigma Fe^{\text{Möss-EPMA}}$ and Cr# were strongly correlated. We explain the rationale for this procedure in the discussion.

Results

Compositions of the Wood spinels and selection of correction and validation standards

We present the uncorrected EPMA analyses of the 32 Wood spinels in Table 2. We used these measurements to look for compositional systematics in the entire set of Wood spinels and to select the samples for the correction and validation sets. Figure 1 shows uncorrected $Fe^{3+}/\Sigma Fe$ ratios determined by EPMA compared to $Fe^{3+}/\Sigma Fe$ ratios determined by Mössbauer (Wood and Virgo 1989; Bryndzia and Wood 1990; Ionov and Wood 1992). The uncorrected $Fe^{3+}/\Sigma Fe$ ratios determined by EPMA analysis correlate with the $Fe^{3+}/\Sigma Fe$ ratios determined by Mössbauer spectroscopy ($r^2 = 0.86$). The whole data set fits the 1:1 line well; however, closer inspection reveals that agreement between the two methods varies from session to session. For example, analyses from session S1 plot consistently above the 1:1 line, and analyses from session S3 plot below. This underscores the assessment of Wood and Virgo (1989) that EPMA is sufficiently precise, but insufficiently accurate to be used without correction. Among the Wood spinels, we

find no systematic relationship in the sample average compositions between the Cr# of the spinels and their $Fe^{3+}/\Sigma Fe$ ratio, but Cr# and MgO (r^2=0.93) are negatively correlated (Figure 2).

From the Wood spinels, we selected seven samples for the correction set and six samples for the validation set. These samples are indicated in Table 2. The selection criteria for the correction and validation sets are given in the Supplementary Material.

Uncorrected and corrected $Fe^{3+}/\Sigma Fe$ ratios of the validation set spinels

Compositions of the validation set spinels were determined by averaging the replicate analyses from analytical sessions A1-A4 and B1-B4 (Table 4). Full results of all analytical sessions are presented in the Supplementary Material (Supplementary Table S2). Figure 3 shows several illustrative examples of uncorrected and corrected $Fe^{3+}/\Sigma Fe$ ratios of the correction and validation set spinels compared with $Fe^{3+}/\Sigma Fe$ ratios determined by Mössbauer, and Figure 4 shows the relationship between $\Delta Fe^{3+}/\Sigma Fe^{Möss\text{-}EPMA}$ and Cr# from these sessions. Below, we discuss the implications of these results for the accuracy and precision of spinel $Fe^{3+}/\Sigma Fe$ ratios determined by EPMA.

Discussion

Accuracy and Precision of the correction method

Since the Wood group presented their correction method and measurements of spinel peridotite f_{O2} (Wood and Virgo 1989; Bryndzia and Wood 1990; Ionov and Wood 1992), the application of this correction method to spinel peridotite f_{O2} studies has been sporadic. Some groups adopted the Wood and Virgo (1989) approach (e.g., Ionov and Wood 1992; Woodland et al. 1992; Luhr and Aranda-Gómez 1997; Parkinson and Pearce 1998; Parkinson and Arculus 1999; Bryant et al.

222 2007; Wang et al. 2007, 2008; Dare et al. 2009), while others presented data with no correction
223 (e.g., Ballhaus 1993; Qi et al. 1995; Fedortchouk et al. 2005; Canil et al. 2006; Foley et al. 2006;
224 Nasir et al. 2010; Wang et al. 2012).

225 Ballhaus et al. (1991) questioned whether $Fe^{3+}/\Sigma Fe$ ratios determined from EPMA require
226 correction, and additionally suggested that such a correction may introduce additional error.
227 Their argument was based in part on a compilation of $\log f_{O2}$ calculated from analyses of spinels
228 in peridotites and basalts, including spinel $Fe^{3+}/\Sigma Fe$ ratios that had been measured both by
229 Mössbauer spectroscopy and EPMA. They found that differences in calculated f_{O2} seldom varied
230 by greater than 0.4 log units and concluded that correcting EPMA data was unnecessary;
231 however, plotting calculated $\log f_{O2}$ rather than spinel $Fe^{3+}/\Sigma Fe$ ratios disguises the true effects of
232 the uncertainty in the EPMA measurements. Uncertainty in spinel $Fe^{3+}/\Sigma Fe$ ratio has a
233 decreasing influence on calculated f_{O2} as $Fe^{3+}/\Sigma Fe$ ratio increases (Ballhaus et al. 1991;
234 Parkinson and Arculus 1999). Plotting $Fe^{3+}/\Sigma Fe$ ratios determined by EPMA and Mössbauer
235 across several studies of natural spinels (Figure 5) shows that disagreement between the two
236 methods can be substantial. In aggregate, the uncorrected $Fe^{3+}/\Sigma Fe$ ratios from previous studies
237 (Figure 5a) are offset to low $Fe^{3+}/\Sigma Fe$ ratios compared to Mössbauer ($\Delta Fe^{3+}/\Sigma Fe^{\text{Möss-EPMA}}$ =
238 0.022±0.049, 1σ). This may indicate a common analytical bias between laboratories. Bias to low
239 values of uncorrected $Fe^{3+}/\Sigma Fe$ ratios could be caused by an overestimate of cations with valence
240 ≥3 or an underestimate of cations with valence ≤2. Possible sources of this bias include treating
241 all Cr as trivalent when a significant fraction may be divalent (Lucas et al. 1988) and omission of
242 divalent minor cations, such as Zn, from the analysis. Corrected $Fe^{3+}/\Sigma Fe$ ratios from these same
243 studies are in closer agreement with Mössbauer $Fe^{3+}/\Sigma Fe$ ratios and are more evenly distributed

around the linear trend between the two measurements ($\Delta Fe^{3+}/\Sigma Fe^{Möss\text{-}EPMA}$ = -0.007±0.021, 1σ; Figure 5b).

Ballhaus et al. (1991) also argued that EPMA analyses of spinel should be corrected only if non-stoichiometry is suspected. But the Wood and Virgo (1989) correction does not imply non-stoichiometry of the spinel sample; it corrects for error in the determination of $Fe^{3+}/\Sigma Fe$ ratios that results from forcing an imperfectly analyzed composition into a perfect stoichiometric calculation. The corrected compositions in this study are still stoichiometric (Supplementary Table S2) with total cations between 2.99 and 3.01 when calculated on a four oxygen basis.

We tested the accuracy and precision of the W&V89 correction using our replicate analyses of spinels from the validation set, BMRG08-98-2-2, and Hawaiian xenoliths analyzed in sessions A1-A4 and B1-B4 (Supplementary Table S2, Figures 3 and 4). If we assume that the Mössbauer analyses of the Wood spinels accurately represent their $Fe^{3+}/\Sigma Fe$ ratios, then we can use the validation set to demonstrate that the W&V89 correction improves the accuracy of $Fe^{3+}/\Sigma Fe$ ratios determined by EPMA. Figure 6 shows the averages and 1σ ranges of both corrected and uncorrected $Fe^{3+}/\Sigma Fe$ ratios of the validation set spinels measured across all analytical sessions (Table 4). Corrected $Fe^{3+}/\Sigma Fe$ ratios are distributed closely around the 1:1 line with an average offset of +0.004 from the Mössbauer $Fe^{3+}/\Sigma Fe$ ratios. The uncorrected $Fe^{3+}/\Sigma Fe$ ratios of these spinels are offset below the 1:1 line by an average of -0.031 from the Mössbauer $Fe^{3+}/\Sigma Fe$ ratios. Similar to the offset in the literature data described above (Figure 5a).

We can assess the improvement in precision of $Fe^{3+}/\Sigma Fe$ ratios achieved by using the W&V89 correction by quantifying the intersession variability of $Fe^{3+}/\Sigma Fe$ ratios that we calculated for the validation set spinels. Values of 1σ around mean uncorrected $Fe^{3+}/\Sigma Fe$ ratios of the validation set

spinels vary from ±0.029 to ±0.065 (Table 4) with a mean of ±0.049. Values of 1σ around mean corrected $Fe^{3+}/\Sigma Fe$ ratios of the validation set spinels vary from ±0.012 to ±0.032 (Table 4) with a mean of ±0.023, which suggests greater than a factor of two increase in precision when using the W&V89 correction. The variations in 1σ around these averages are not random. Intersession variability in corrected and uncorrected $Fe^{3+}/\Sigma Fe$ ratios is greater in samples with lower total Fe. The stoichiometric calculation produces a concentration of Fe^{3+} with uncertainty resulting from the accumulated analytical errors from each element propagated through the stoichiometric calculation. When this error is propagated through the calculation of the $Fe^{3+}/\Sigma Fe$ ratio, it scales with the total concentration of Fe. We approximate errors on corrected $Fe^{3+}/\Sigma Fe$ ratios by dividing the error on Fe^{3+} by the amount of total Fe. We demonstrate this relationship by plotting the magnitude of 1σ variations in corrected $Fe^{3+}/\Sigma Fe$ ratios from validation set and Hawaiian spinels as a function of the inverse of total Fe per 3 formula cations (Figure 7a). A line fit through the origin gives the following relationship:

$$1\sigma_3 = 0.006/X_{\Sigma Fe} \quad (3)$$

where $1\sigma_3$ describes the magnitude of one standard deviation around a corrected spinel $Fe^{3+}/\Sigma Fe$ ratio, 0.006 is the magnitude of 1σ variation around the mean molar Fe^{3+} concentration per 3 formula cations, and $X_{\Sigma Fe}$ is the molar concentration of total Fe per 3 formula cations. This relationship describes an error envelope for corrected $Fe^{3+}/\Sigma Fe$ ratios that depends on the total concentration of Fe in the spinel. Figure 7b shows the error envelope with measurements of $Fe^{3+}/\Sigma Fe$ ratios from the validation set, Hawaiian, and Tongan spinels presented as deviations from the mean. Equation 3 describes the precision of the EPMA method of determining $Fe^{3+}/\Sigma Fe$ ratios when using the W&V89 correction.

It is likely that the accuracy of uncorrected $Fe^{3+}/\Sigma Fe$ ratios and the precision of $Fe^{3+}/\Sigma Fe$ ratios corrected using the W&V89 method can be improved further by analyzing additional minor elements. As we described above, our uncorrected spinel $Fe^{3+}/\Sigma Fe$ ratios measured by EPMA and those in previous studies skew low compared to Mössbauer $Fe^{3+}/\Sigma Fe$ ratios, consistent with under-sampling of divalent cations. We examined the spinel dataset hosted in the GEOROC database (http://georoc.mpch-mainz.gwdg.de/georoc/, accessed 30 June 2016). In 139 peridotite-hosted spinels (those with host rock listed as peridotite, lherzolite, harzburgite, or dunite) with both major and trace first-row transition elements given, only three transition elements have average concentrations in excess of 100 ppm: V (620±390), Co (270±220), and Zn (960±690). Forty-two of these samples have measured V, Co, and Zn, and in that subset V is positively correlated with both Co ($r^2 = 0.54$) and Zn ($r^2 = 0.33$; Supplementary Figure S1). In all but 4 of these spinel samples (Co+Zn) is greater than V; therefore, it is likely that by excluding these elements from the analysis, we have introduced a bias that could lead to uncorrected $Fe^{3+}/\Sigma Fe$ ratios that are underestimated by 0.003 to 0.013 (see Supplementary Materials for calculations). The W&V89 correction accounts for the systematic underestimation of $Fe^{3+}/\Sigma Fe$, but variations in V, Co, and Zn in standard and unknown spinels may lead to diminished precision of the corrected $Fe^{3+}/\Sigma Fe$ ratios on the order of 0.01 if these elements are not analyzed.

Underlying mechanics of the Wood and Virgo Correction

Although the W&V89 correction demonstrably improves agreement between measurements of spinel $Fe^{3+}/\Sigma Fe$ ratios by Mössbauer and EPMA, no studies by the Wood group nor any subsequent studies have explained how the method works in detail. Wood and Virgo (1989) report that $\Delta Fe^{3+}/\Sigma Fe^{Möss\text{-}EPMA}$ is generally linearly related to Cr#; they suggest a simple linear relationship can be determined in each EPMA analytical session by comparing EPMA analyses

311 of a set of spinel standards that have been characterized by Mössbauer. We explore two
312 complications in this section: 1. How should correction proceed when this linear relationship is
313 not observed, even when agreement between EPMA and Mössbauer measurements of the
314 standards is poor? 2. How does this correction, based only on two measured elements, work to
315 correct a multi-element analysis? The first question was raised by Luhr and Aranda-Gomez
316 (1997), who reported that their EPMA measurments of spinel $\Delta Fe^{3+}/\Sigma Fe^{Möss\text{-}EPMA}$ and Cr# were
317 not correlated. We also do not observe a correlation between $\Delta Fe^{3+}/\Sigma Fe^{Möss\text{-}EPMA}$ and Cr# in
318 some of our analytical sessions (e.g., Session B4, Figure 4). The second question was addressed
319 briefly by Wood and Virgo (1989), who suggested that Al was subject to greater systematic
320 errors than other elements, at least in their own data set; therefore a correction relying on Cr#
321 addressed the greatest source of uncertainty. As we demonstrate below, systematic error of any
322 element in the EPMA analysis can lead to increases in the magnitude of $\Delta Fe^{3+}/\Sigma Fe^{Möss\text{-}EPMA}$, but
323 the W&V89 correction can still correct for these biases. That is, the correction works, even
324 when bias is introduced by elements other than Cr or Al, largely because of a correlation
325 between Cr# and MgO in the global spinel peridotite data set (Figure 8); however, this means
326 that the correction may be less effective for samples that fall off the MgO-Cr# trend. This aspect
327 of the W&V89 correction needs to be accounted for by workers analyzing off-trend spinels,
328 either by adjusting estimates of uncertainty or by choosing correction standards that are
329 compositionally relevant to their particular sample set.

330 Biases in EPMA can lead to two different effects on calculated $Fe^{3+}/\Sigma Fe$ ratios of a group of
331 spinels for which independent Mössbauer $Fe^{3+}/\Sigma Fe$ ratios are available. The whole set of EPMA-
332 derived $Fe^{3+}/\Sigma Fe$ ratios may be offset from the EPMA-Mössbauer 1:1 line. Alternatively, scatter
333 around the linear trend between Mössbauer and EPMA $Fe^{3+}/\Sigma Fe$ ratios may increase as spinels

with different compositions are variably affected by measurement bias. These two effects are not mutually exclusive.

When the correction set yields a constant offset (e.g., Sessions B1 and B4, Figure 3e), uncorrected $Fe^{3+}/\Sigma Fe$ ratios of the correction and validation set spinels plot mostly below the 1:1 line and $\Delta Fe^{3+}/\Sigma Fe^{Möss\text{-}EPMA}$ and Cr# are also uncorrelated ($r^2 \leq 0.10$; Figure 4c). In such instances, EPMA-derived $Fe^{3+}/\Sigma Fe$ ratios display systematic bias, but it is not clear that a correction scheme that relies on a correlation between $\Delta Fe^{3+}/\Sigma Fe^{Möss\text{-}EPMA}$ and Cr# should be applied when those parameters are uncorrelated. Luhr and Arranda-Gomez (1997) observed just such a scenario when they attempted to apply the W&V89 correction to their own spinel peridotite xenolith suite. They chose not to apply the W&V89 correction and instead determined the average value of $\Delta Fe^{3+}/\Sigma Fe^{Möss\text{-}EPMA}$ for all their correction standards, which did not vary with Cr#. They then made a single, constant-value adjustment to the calculated $Fe^{3+}/\Sigma Fe$ ratio of all samples run during that session. This method of correction can improve $Fe^{3+}/\Sigma Fe$ ratio accuracy in the case where the offset between EPMA and Mössbauer is roughly constant for all samples; however, devising a separate correction for such a case is unnecessary. The W&V89 correction contains this same functionality: when $\Delta Fe^{3+}/\Sigma Fe^{Möss\text{-}EPMA}$ and Cr# are uncorrelated, the slope of the best fit line will be approximately zero, and the W&V89 correction functions as a constant $Fe^{3+}/\Sigma Fe$ ratio offset correction. The two correction methods are, in effect, equivalent.

The W&V89 correction is valuable because it addresses the differential effects of measurement bias on spinels of variable composition. Hence, the correction can also decrease scatter in EPMA measurements of $Fe^{3+}/\Sigma Fe$ ratios when these data show large deviations from the linear trend with $Fe^{3+}/\Sigma Fe$ ratios by Mössbauer. Sessions A3 (Figures 3a and 3b) and B3 are examples of this effect. The initial stoichiometric calculation of spinel $Fe^{3+}/\Sigma Fe$ ratio is sensitive to systematic

errors in all elements analyzed. Wood and Virgo (1989) explain their choice of Cr# as the compositional parameter for correcting $Fe^{3+}/\Sigma Fe$ ratios because, among the major elements, Al_2O_3 concentrations determined by EPMA were the most affected by the choice of matrix correction schemes. This explanation does not account for systematic biases of elements other than Al and Cr that may result from imperfect analysis of primary standards.

MgO is a major element in peridotitic spinels and is just as likely as Al or Cr to be the root of systematic offsets of calculated $Fe^{3+}/\Sigma Fe$ ratios from ideality. Interestingly, the W&V89 correction is able to correct for bias in the MgO analysis because MgO and Cr# are correlated in the spinels studied by the Wood group (Wood and Virgo 1989; Bryndzia and Wood 1990; Ionov and Wood 1992) and in peridotitic spinels globally (Figures 2 and 8). The correlation between MgO and Cr# in peridotitic spinels is an expected consequence of the dependence of the Fe^{2+}-Mg exchange coefficient between olivine and spinel on the Cr concentration in the spinel (Irvine 1965; Wood and Nicholls 1978). This relationship in the spinel data increases the effectiveness of the W&V89 correction when unknown spinel samples overlap with the compositional range of the correction standards, but the correction may not be as effective for samples which fall significantly off that compositional trend. In the Supplementary Materials, we present calculations that demonstrate how the W&V89 correction improves the accuracy of spinel $Fe^{3+}/\Sigma Fe$ ratios when elements other than Cr and Al are biased during the analysis. These calculations also demonstrate that corrected $Fe^{3+}/\Sigma Fe$ ratios from spinels that depart from the MgO-Cr# trend of the correction set, such as Tonga sample BMRG08-98-2-2, are subject to degraded precision.

In summary, the W&V89 correction can effectively correct for systematic biases in EPMA derived $Fe^{3+}/\Sigma Fe$ ratios, even when the correlation between $\Delta Fe^{3+}/\Sigma Fe^{Möss\text{-}EPMA}$ and Cr# is weak

or absent. The W&V89 method also corrects for bias in measured elements other than Al_2O_3 and Cr_2O_3, due predominantly to the correlation of spinel Cr# with MgO. Precision of corrected $Fe^{3+}/\Sigma Fe$ ratios decreases for samples that fall outside the compositional range of the correction standards used, but accuracy is no worse than if the correction had not been applied. This effect could be mitigated by choosing a different set of correction standards that are compositionally similar to the unknowns being analyzed.

Effect of the matrix correction scheme

Wood and Virgo (1989) investigated the effect of the choice of matrix correction schemes on EPMA measurements of spinels. They found that different matrix correction schemes led to systematic differences in the calculated magnetite activity in spinel compositions before applying the W&V89 $Fe^{3+}/\Sigma Fe$ correction. We have reprocessed the analyses from analytical sessions A1-A4 using the PAP matrix correction (Pouchou and Pichoir 1986; Supplementary Table S3), also considered by Wood and Virgo (1989). We find that, compared to the ZAF correction we have used throughout our study, the PAP correction results in systematically lower Al_2O_3 (averaging 1.4% relative), FeO (0.4%), and MgO (0.6%) and systematically higher Cr_2O_3 (0.7%). Uncorrected $Fe^{3+}/\Sigma Fe$ ratios determined using the PAP procedure are 0.001 to 0.015 lower than those ratios determined using the ZAF procedure, and the difference in $Fe^{3+}/\Sigma Fe$ ratio by these two matrix corrections is correlated with Cr# ($r^2 = 0.975$). Despite this systematic offset, the magnitude of the difference in uncorrected $Fe^{3+}/\Sigma Fe$ ratios is small, even in Al-rich samples, compared to the variation caused by session-to-session differences in the primary standardization. After correcting the $Fe^{3+}/\Sigma Fe$ ratios using the W&V89 method, the PAP and ZAF procedures yield differences in $Fe^{3+}/\Sigma Fe$ (ZAF-PAP) between -0.002 and 0.001. When the W&V89 correction is used, effects of the matrix correction on the $Fe^{3+}/\Sigma Fe$ ratio are negligible.

Calculation of f_{O2} from the analyses of spinel, olivine, and orthopyroxene

Ultimately, the goal of determining the $Fe^{3+}/\Sigma Fe$ ratios of spinels from peridotites is to estimate the f_{O2} of equilibration. We calculate f_{O2} following Mattioli and Wood (1988) and Wood and Virgo (1989) using the following equation for $\log f_{O2}$:

$$\log (f_{O_2})_{P,T} = \frac{-24222}{T} + 8.64 + \frac{0.0567P}{T} - 12\,log(1 - Mg\#^{ol}) - \frac{2620}{T}(Mg\#^{ol})^2$$

$$+3\log(\mathrm{X}_{Fe}^{M1} \cdot \mathrm{X}_{Fe}^{M2})^{opx} + 2\log\,(a_{Fe_3O_4}^{spl}) \qquad (4)$$

where P is pressure in bars, T is temperature in K, $Mg\# = X_{Mg}^{ol}/(X_{Mg}^{ol} + X_{Fe}^{ol})$, and X_{Mg}^{ol}, X_{Fe}^{ol} are the mole fractions of Mg and Fe in olivine, X_{Fe}^{M1} and X_{Fe}^{M2} are the mole fractions of Fe in the two orthopyroxene octahedral sites calculated following Wood and Banno (1973), and $a_{Fe_3O_4}^{spl}$ is the activity of the magnetite component in spinel. We discuss the calculation of $a_{Fe_3O_4}^{spl}$ in the following section. Temperature and pressure are required to calculate f_{O2}. We calculate temperature using the spinel-olivine Fe-Mg exchange thermometer of Li et al. (1995) and, unless otherwise specified, we follow Bryndzia and Wood (1990) and Wood et al. (1990) in assuming a pressure of 1.5 GPa.

Equation 4 does not appear in the above form in any of the Wood group papers, and there is some confusion in the literature about how different versions of the formula arose. Commonly, the version given in Wood et al. (1990) and Wood (1991) is cited, which includes a term for the f_{O2} of the quartz-fayalite-magnetite (QFM) buffer:

$$\log (f_{O_2})_{P,T} = \log\big(f_{O_2}\big)_{P,T}^{QFM} + \frac{220}{T} + 0.35 - \frac{0.0369P}{T} - 12\,log(1 - Mg\#^{ol})$$

$$-\frac{2620}{T}(Mg\#^{ol})^2 + 3\log(\mathrm{X}_{Fe}^{M1} \cdot \mathrm{X}_{Fe}^{M2})^{opx} + 2log\ a_{Fe_3O_4}^{spl} \quad (5)$$

As discussed by Herd (2008), this version of the f_{O2} equation requires the QFM formulation of Myers and Eugster (1983):

$$logf_{O_2}(QFM)_{1bar,T} = \frac{-24441.9}{T} + 8.29 \quad (6)$$

(Subtracting eq. 6 from the first two terms in eq. 4 yields the second two terms in eq. 5.) Herd (2008) also suggests that the proper way to calculate absolute f_{O2} from eq. 5 is to use eq. 6 as written, without a pressure term, to calculate $logf_{O_2}(QFM)_{P,T}$. This is incorrect because the pressure term in eq. 5 is derived from the difference between the pressure dependences of the spinel-olivine-orthopyroxene buffer and QFM. Mattioli and Wood (1988) describe a method by which the pressure dependence of the spinel-olivine-orthopyroxene buffer can be approximated from standard state molar volumes of the phases by assuming Mg# = 0.90 in each of the silicates and a magnetite proportion of 0.02 in spinel. The resulting coefficient ($\Delta V/(2.303*R)$ = 0.0567) appears in both Wood and Virgo (1989) and Bryndzia and Wood (1990). From this, we can determine the P/T coefficient in eq. 5 by subtracting the pressure dependence of the QFM buffer ($\Delta V/(2.303*R)$ = 0.0936, using the standard state molar volumes given in Robie, Hemingway, et al. 1995) from eq. 4.

Using eq. 6 to calculate $logf_{O_2}(QFM)_{P,T}$ for use in eq. 5 with no pressure term leads to a 0.6 log unit underestimation of absolute f_{O2} at 1150 °C and 1 GPa. Substituting a parameterization of QFM into eq. 5 other than that of Myers and Eugster (1983) leads to systematic errors in f_{O2}. For example, replacement with O'Neill (1987) results in a 0.15 log unit underestimation of absolute f_{O2} at 1150 °C and 1 GPa. We avoid this confusion by using eq. 4 to calculate $\log\ (f_{O_2})_{P,T}$

before calculating f_{O2} relative to the QFM reference buffer. Except where otherwise indicated, we report oxygen fugacity relative to QFM using the parameterization of Frost (1991):

$$log f_{O_2}(QFM)_{1bar,T} = \frac{-25096.3}{T} + 8.735 + \frac{0.11(P-1)}{T} \quad (7)$$

We calculate magnetite activity in spinel, $a_{Fe_3O_4}^{spl}$ using the MELTS Supplemental Calculator (Sack and Ghiorso 1991a, 1991b; http://melts.ofm-research.org/CalcForms/index.html) with a slight modification to the calculation of spinel components. We describe this modification and justify our choice of the MELTS Supplemental Calculator for calculating $a_{Fe_3O_4}^{spl}$ in the Supplementary Materials.

Uncertainty in the f_{O2} calculation contributed by the EPMA analysis

Uncertainty in f_{O2} calculated from spinel peridotite oxybarometry depends on the accuracy and precision of the three compositional variables in eq. 4, $Mg\#^{ol}$, $(X_{Fe}^{M1} \cdot X_{Fe}^{M2})^{opx}$, and $a_{Fe_3O_4}^{spl}$, resulting from analysis by EPMA as well as on the uncertainty in the temperature and pressure of equilibration. We estimated uncertainty contributed by the compositional terms from repeated analysis of secondary standards. The uncertainty in f_{O2} from the olivine analysis increases with $Mg\#^{ol}$ from ±0.04 log units at $Mg\#^{ol}$=0.85 to ±0.14 log units at $Mg\#^{ol}$=0.95, and the orthopyroxene analysis contributes an additional ±0.04 log units. We provide a complete description of how these uncertainties were calculated in the Supplementary Material.

We are able to relate uncertainty in the calculation of spinel $Fe^{3+}/\Sigma Fe$ ratios to uncertainty in $\log(a_{Fe_3O_4}^{spl})$ calculated from the MELTS Supplemental Calculator through a logarithmic relationship described in the Supplementary Material (Supplementary Figure S4). Following

462 Parkinson and Arculus (1999) and Ballhaus et al., (1991), Figure 9a shows the relationship
463 between $\log\left(a_{Fe_3O_4}^{spl}\right)$ and relative f_{O2}, and Figure 9b shows how relative f_{O2} varies with spinel
464 $Fe^{3+}/\Sigma Fe$ ratio. The uncertainty in relative f_{O2} contributed by the spinel analysis is asymmetrical
465 and increases with decreasing $Fe^{3+}/\Sigma Fe$ ratio. At $Fe^{3+}/\Sigma Fe = 0.10$ the error in f_{O2} is $^{+0.3}_{-0.4}$ log units
466 (1σ), while at $Fe^{3+}/\Sigma Fe = 0.35$ the error is ±0.1 log units (Figure 9b). Figure 9 also shows an
467 error envelope for the precision of the $Fe^{3+}/\Sigma Fe$ ratio measurement with no correction (dotted
468 lines). Uncertainty in $\log\left(a_{Fe_3O_4}^{spl}\right)$ approximately doubles for spinel analyses that have not been
469 corrected using the W&V89 method. This is particularly important for spinels with $Fe^{3+}/\Sigma Fe$
470 ratios < 0.10, which may have uncertainties in f_{O2} in excess of a log unit when uncorrected.

471 Temperature and pressure both enter into the calculation of f_{O2} from spinel-olivine-
472 orthopyroxene equilibria and must be determined through thermobarometry, or some suitable
473 temperature and pressure must be assumed. We have calculated equilibration temperatures of the
474 Hawaiian xenoliths using the spinel-olivine Fe-Mg exchange thermometer of Li et al. (1995),
475 and we assume a pressure of 1.5 GPa. Li et al. (1995) did not evaluate the standard error of their
476 thermometer using an independent validation data set, so we estimated uncertainty from the
477 standard deviation in our own measurements of the Hawaiian xenoliths. For each Hawaiian
478 xenolith, we calculated temperatures from the average spinel composition from each analytical
479 session (Supplementary Table S2) and the sample average olivine compositions in Table 3. The
480 standard deviation in calculated temperature for these samples varies from 25 to 82 °C. To be
481 conservative, we used ±80 °C as our temperature uncertainty to explore the effects of
482 temperature error on the f_{O2} calculation.

The effect of temperature on calculated f_{O2} is compositionally dependent as temperature enters into the f_{O2} calculation both explicitly in eq. 4 and in the calculation of $a^{spl}_{Fe_3O_4}$. Increasing temperature leads to a decrease in calculated f_{O2} relative to QFM, but this effect is greater when spinel Cr# is lower (Supplementary Figure S5). The magnitude of uncertainty due to temperature is also a function of temperature, such that samples with colder equilibration temperatures have greater uncertainty in f_{O2}. The temperature uncertainty of ±80 °C contributes about ±0.1 log units of uncertainty to the f_{O2} calculated for low-Cr# sample 114923-41 at its calculated equilibration temperature (1118 °C). Temperature uncertainty for a similar peridotite with a colder equilibration temperature of 700 °C (e.g., as appropriate for supra-subduction zone peridotites; Parkinson and Pearce 1998), would contribute >0.2 log units of uncertainty to the f_{O2} calculation.

Pressure is not well-constrained for spinel peridotites due to the absence of a strongly pressure dependent reaction (MacGregor 2015). It is common for spinel peridotite oxybarometry studies to assume a single pressure for the f_{O2} calculation (e.g., Bryndzia and Wood 1990; Wood et al. 1990; Ballhaus 1993). We follow Wood et al. (1990) in choosing 1.5 GPa, which is roughly the center of the pressure range of spinel stability. Logf_{O2} decreases linearly with increasing pressure (Eq. 4), and each 0.25 GPa of pressure uncertainty leads to about ±0.1 log units uncertainty in f_{O2}.

Hawaiian xenolith f_{O2}

The replicate analyses of the Hawaiian xenoliths allow for an additional check on our estimated uncertainty in the f_{O2} calculation. Figure 10 shows $Fe^{3+}/\Sigma Fe$ ratios, $a^{spl}_{Fe_3O_4}$, and f_{O2} relative to QFM calculated for each individual analysis of each of the Hawaiian spinels. We calculated $a^{spl}_{Fe_3O_4}$ and f_{O2} using the spinel-olivine exchange temperature particular to each spinel analysis.

505 For each sample, measurements of relative f_{O2} from each analytical session fall well within the
506 estimated error from all other measurements of that sample (Fig. 10a). This broad overlap is
507 partly due to the use of only a single measurement of olivine and orthopyroxene from each
508 sample, eliminating two sources of potential variation. Fig. 10b, which shows variation in the
509 calculated $a^{spl}_{Fe_3O_4}$, shows that error bars in $\log a^{spl}_{Fe_3O_4}$ for all measurements of a given sample are
510 also overlapping. This suggests that we have suitably propagated uncertainty in spinel $Fe^{3+}/\Sigma Fe$
511 ratios to uncertainty in $a^{spl}_{Fe_3O_4}$. Although samples with greater spinel $Fe^{3+}/\Sigma Fe$ ratios also record
512 greater f_{O2} relative to QFM, estimates of $a^{spl}_{Fe_3O_4}$ based on independent measurements of any
513 given sample can increase, decrease, or remain constant with increasing spinel $Fe^{3+}/\Sigma Fe$ ratio
514 (Figure 10b). This highlights that the temperature estimation contributes significantly to the
515 calculation of f_{O2}.

516 The four Hawaiian xenoliths analyzed in this study record relative oxygen fugacities between
517 QFM+0.15 $^{+0.34}_{-0.37}$ and QFM+0.98 $^{+0.24}_{-0.25}$ (Table 4, Fig. 10) at their equilibration temperatures
518 and 1.5 GPa, which is slightly more oxidized than the mean f_{O2} recorded by abyssal peridotites
519 from spreading centers (Bryndzia and Wood 1990; Wood et al. 1990). These relative oxygen
520 fugacities also depend on temperature and pressure, and the quoted uncertainties do not reflect
521 the additional uncertainties associated with our choice of pressure and temperature. Further
522 contextualization of these results is beyond the scope of this communication, and will be
523 discussed along with a larger data set in a future publication.

524 **Comparison of the Wood (1991) and Ballhaus et al. (1991) parameterizations of the spinel**
525 **peridotite oxybaromater**

Although we have chosen to use the Wood (1991) version of the spinel-olivine-orthopyroxene oxybarometer to calculate f_{O2} (eq. 4), numerous other studies use the Ballhaus et al. (1991) version of the oxybarometer. These two parameterizations are commonly considered to be interchangeable (e.g., Woodland et al. 1992; Ballhaus 1993; Canil et al. 2006). Herd (2008) demonstrated that relative f_{O2} calculated using the Ballhaus et al. (1991) method is systematically lower than relative f_{O2} calculated with the Wood (1991) method. Luhr and Arranda-Gomez (1997) similarly found that f_{O2} calculated using Ballhaus et al. (1991) was on average 0.8 log units below those calculated using Wood (1991). We compare the two parameterizations in Fig. 10c using the Hawaiian xenolith data. Results from the two methods are correlated (r^2=0.82). Consistent with Herd (2008), relative f_{O2} calculated using the Ballhaus et al. (1991) method is 0.7 to 1.3 log units lower than results from the Wood (1991) method. The two methods cannot be considered directly comparable, and comparisons of peridotite f_{O2} data between studies using different f_{O2} parameterizations requires that sufficient analytical data be provided to allow for recalculation using either method.

Implications

The precision of f_{O2} calculated from spinel peridotite oxybarometry is chiefly limited by the precision of the measurement of spinel $Fe^{3+}/\Sigma Fe$ ratios. We have shown that flaws in the primary standardization are the greatest source of imprecision in spinel $Fe^{3+}/\Sigma Fe$ ratios determined by EPMA and that maximizing the precision of spinel $Fe^{3+}/\Sigma Fe$ ratios requires the use of correction standards with independently measured $Fe^{3+}/\Sigma Fe$ ratios. The W&V89 correction leads to a 2-fold improvement in precision of $Fe^{3+}/\Sigma Fe$ ratios for most spinels measured by EPMA, and further improvements are possible if common minor elements such as V, Co, and Zn are also analyzed.

548 The f_{O2} recorded by peridotites offers insight into f_{O2} conditions prevalent in Earth's upper
549 mantle. If spinel peridotite oxybarometry is used to detect f_{O2} variations between different
550 tectonic environments (e.g., Ballhaus 1993) or between different samples from a local
551 environment, then measurements that allow the f_{O2} recorded by peridotites to be calculated must
552 be more precise than the range of f_{O2} recorded by these samples. Uncertainty in calculated f_{O2}
553 contributed by uncorrected EPMA analyses of spinel $Fe^{3+}/\Sigma Fe$ ratios may be greater than ±1 log
554 units (1σ) at f_{O2} less than about QFM-1 (Figure 9). For comparison, the entire abyssal peridotite
555 suite of Bryndzia and Wood (1990) varies in f_{O2} by only ±0.7 log units (1σ). We recommend that
556 future studies that present EPMA measurements of spinel $Fe^{3+}/\Sigma Fe$ ratio use the W&V89
557 method, or at least include analyses of spinel standards with independently measured $Fe^{3+}/\Sigma Fe$
558 ratios so that precision may be estimated. Publication of complete EPMA data sets collected on
559 unknowns and standards should become standard practice for spinel oxybarometry studies.

560 We have also provided methods for quantifying the contributions to total uncertainty in
561 calculated f_{O2} from each parameter in the oxybarometer. For spinels with relatively low $Fe^{3+}/\Sigma Fe$
562 ratios, the greatest contribution to this uncertainty comes from the calculation of $a_{Fe_3O_4}^{spl}$, which is
563 directly tied precision of measured $Fe^{3+}/\Sigma Fe$ ratios in spinel. This precision is dependent on the
564 total concentration of Fe in the spinel and on the $Fe^{3+}/\Sigma Fe$ ratio itself. The difference in
565 uncertainty in calculated f_{O2} from corrected spinel analyses compared to uncorrected analyses is
566 lower by >0.5 log units for spinels with $Fe^{3+}/\Sigma Fe$ ratios < 0.10.

567 Several studies have found evidence for differences in f_{O2} recorded by peridotites from different
568 tectonic environments. Wood et al. (1990) found that the average f_{O2} recorded by continental
569 xenoliths was about one order of magnitude greater than the average of abyssal peridotites (QFM

570 -1; Bryndzia and Wood 1990). Ballhaus (1993) found that xenoliths from OIB localities were
571 also on average about one log unit more oxidized than abyssal peridotites. Parkinson and Arculus
572 (1999) showed that subduction-related peridotites record average f_{O2} of approximately QFM+1,
573 about 2 log units more oxidized than abyssal peridotites. These differences of 1-2 log units are
574 small enough that uncorrected EPMA data or calculations of f_{O2} using different formulations,
575 may be too imprecise to resolve them.

576 Analysis of peridotite f_{O2} provides an alternative perspective on the f_{O2} prevalent in different
577 upper mantle settings that complements the variations in f_{O2} revealed by analyses of basaltic
578 glasses (Kelley and Cottrell 2012). In tectonic settings where f_{O2} has been estimated from both
579 peridotites and glasses the results can be incongruent, which may indicate that, in addition to
580 inherent differences between tectonic settings, f_{O2} records are subject to petrological processes in
581 the upper mantle (e.g., Birner et al. 2016). For example, abyssal peridotites suggest a MORB
582 source region with average f_{O2} of QFM-1 (Bryndzia and Wood 1990), but MORB glasses
583 suggest a more oxidized MORB source with average f_{O2} of QFM (Cottrell and Kelley 2011).
584 Future measurements of f_{O2} of mid-ocean ridge peridotites will need to use the W&V89
585 correction to achieve sufficient precision to allow an investigation of the potential petrological
586 causes for this incongruence.

587 Finally, the greatest advantage that EPMA holds over Mössbauer analysis is that it allows spinel
588 $Fe^{3+}/\Sigma Fe$ ratios to be easily measured at the micrometer scale. As we try to connect f_{O2}
589 measurements in peridotites to petrological processes, it may become necessary to investigate
590 variations in spinel $Fe^{3+}/\Sigma Fe$ ratios at the grain scale. Changes in the $Fe^{3+}/\Sigma Fe$ ratio between
591 spinel cores and rims, for example, can be observed by accurate and precise EPMA
592 measurements.

Acknowledgements

The authors thank Bernard Wood for providing spinel samples. We thank Leslie Hale for assisting with access to the Hawaiian xenolith samples from the National Rock and Ore Collection at the National Museum on Natural History (NMNH) in Washington, DC. Chris MacLeod and Sherm Bloomer are thanked for providing access to the Tonga sample. We also wish to thank Tim Gooding and Tim Rose for assistance with sample preparation and for providing expertise and maintaining the electron microprobe lab at NMNH. This paper was improved by constructive reviews from B. Wood and an anonymous reviewer. FD received support from the Smithsonian Peter Buck Fellowship. SB received support from the Stanford Graduate Fellowship and McGee Grant. OL received support from the Natural History Research Experiences NSF REU program (EAR-1062692). We gratefully acknowledge funding from NSF awards OCE-1433212 (to EC) and OCE-1434199 (to JW).

References

Arai, S., and Matsukage, K. (1996) Petrology of gabbro-troctolite-peridotite complex from Hess Deep, equatorial Pacific: implications for mantle-melt interaction within the oceanic lithosphere. In PROCEEDINGS-OCEAN DRILLING PROGRAM SCIENTIFIC RESULTS pp. 135–156. NATIONAL SCIENCE FOUNDATION.

Ballhaus, C. (1993) Redox states of lithospheric and asthenospheric upper mantle. Contributions to Mineralogy and Petrology, 114, 331–348.

612 Ballhaus, C., Berry, R., and Green, D. (1991) High pressure experimental calibration of the
613 olivine-orthopyroxene-spinel oxygen geobarometer: implications for the oxidation state
614 of the upper mantle. Contributions to Mineralogy and Petrology, 107, 27–40.

615 Bézos, A., and Humler, E. (2005) The Fe 3+/ΣFe ratios of MORB glasses and their implications
616 for mantle melting. Geochimica et Cosmochimica Acta, 69, 711–725.

617 Birner, S.K., Warren, J.M., Cottrell, E., and Davis, F.A. (2016) Hydrothermal alteration of
618 seafloor peridotites does not influence oxygen fugacity recorded by spinel oxybarometry.
619 Geology, G38113–1.

620 Bloomer, S., Wright, D., MacLeod, C., Tappin, D., Clift, P., Falloon, T., Fisher, R., Gillis, K.,
621 Ishii, T., Kelman, M., and others (1996) Geology of the Tonga forearc: a supra-
622 subduction zone ophiolite. Eos Trans. AGU, 77, 325.

623 Bonatti, E., Peyve, A., Kepezhinskas, P., Kurentsova, N., Seyler, M., Skolotnev, S., and
624 Udintsev, G. (1992) Upper mantle heterogeneity below the Mid-Atlantic Ridge, 0–15 N.
625 Journal of Geophysical Research: Solid Earth, 97, 4461–4476.

626 Bonatti, E., Seyler, M., and Sushevskaya, N. (1993) A cold suboceanic mantle belt at the Earth's
627 equator. Science, 261, 315–320.

628 Brunelli, D., and Seyler, M. (2010) Asthenospheric percolation of alkaline melts beneath the St.
629 Paul region (Central Atlantic Ocean). Earth and Planetary Science Letters, 289, 393–405.

630 Brunelli, D., Cipriani, A., Ottolini, L., Peyve, A., and Bonatti, E. (2003) Mantle peridotites from
631 the Bouvet triple junction region, south Atlantic. Terra Nova, 15, 194–203.

632 Bryant, J., Yogodzinski, G., and Churikova, T. (2007) Melt-mantle interactions beneath the
633 Kamchatka arc: Evidence from ultramafic xenoliths from Shiveluch volcano.
634 Geochemistry, Geophysics, Geosystems, 8.

635 Bryndzia, L.T., and Wood, B.J. (1990) Oxygen thermobarometry of abyssal spinel peridotites:
636 the redox state and C–O–H volatile composition of the Earth's sub-oceanic upper mantle.
637 American Journal of Science, 290, 1093–1116.

638 Buddington, A., and Lindsley, D. (1964) Iron-titanium oxide minerals and synthetic equivalents.
639 Journal of petrology, 5, 310–357.

640 Canil, D. (1999) Vanadium partitioning between orthopyroxene, spinel and silicate melt and the
641 redox states of mantle source regions for primary magmas. Geochimica et Cosmochimica
642 Acta, 63, 557–572.

643 Canil, D., Virgo, D., and Scarfe, C.M. (1990) Oxidation state of mantle xenoliths from British
644 Columbia, Canada. Contributions to Mineralogy and Petrology, 104, 453–462.

645 Canil, D., Johnston, S.T., and Mihalynuk, M. (2006) Mantle redox in Cordilleran ophiolites as a
646 record of oxygen fugacity during partial melting and the lifetime of mantle lithosphere.
647 Earth and Planetary Science Letters, 248, 106–117.

648 Cannat, M., Bideau, D., and Bougault, H. (1992) Serpentinized peridotites and gabbros in the
649 Mid-Atlantic Ridge axial valley at 15 37′ N and 16 52′ N. Earth and Planetary Science
650 Letters, 109, 87–106.

651 Christie, D.M., Carmichael, I.S., and Langmuir, C.H. (1986) Oxidation states of mid-ocean ridge
652 basalt glasses. Earth and Planetary Science Letters, 79, 397–411.

653 Cipriani, A., Bonatti, E., Brunelli, D., and Ligi, M. (2009) 26 million years of mantle upwelling
654 below a segment of the Mid Atlantic Ridge: The Vema Lithospheric Section revisited.
655 Earth and Planetary Science Letters, 285, 87–95.

656 Constantin, M., Hékinian, R., Ackermand, D., and Stoffers, P. (1995) Mafic and ultramafic
657 intrusions into upper mantle peridotites from fast spreading centers of the Easter
658 Microplate (South East Pacific). In Mantle and lower crust exposed in oceanic ridges and
659 in ophiolites pp. 71–120. Springer.

660 Coogan, L.A., Thompson, G., MacLeod, C.J., Dick, H., Edwards, S., Scheirer, A.H., and Barry,
661 T.L. (2004) A combined basalt and peridotite perspective on 14 million years of melt
662 generation at the Atlantis Bank segment of the Southwest Indian Ridge: evidence for
663 temporal changes in mantle dynamics? Chemical Geology, 207, 13–30.

664 Cottrell, E., and Kelley, K.A. (2011) The oxidation state of Fe in MORB glasses and the oxygen
665 fugacity of the upper mantle. Earth and Planetary Science Letters, 305, 270–282.

666 Cottrell, E., Kelley, K.A., Lanzirotti, A., and Fischer, R.A. (2009) High-precision determination
667 of iron oxidation state in silicate glasses using XANES. Chemical Geology, 268, 167–
668 179.

669 Dare, S.A., Pearce, J.A., McDonald, I., and Styles, M.T. (2009) Tectonic discrimination of
670 peridotites using fO 2–Cr# and Ga–Ti–Fe III systematics in chrome–spinel. Chemical
671 Geology, 261, 199–216.

672 D'Errico, M.E., Warren, J.M., and Godard, M. (2016) Evidence for chemically heterogeneous
673 Arctic mantle beneath the Gakkel Ridge. Geochimica et Cosmochimica Acta, 174, 291–
674 312.

675 Dick, H. (1989) Abyssal peridotites, very slow spreading ridges and ocean ridge magmatism.
676 Magmatism in the ocean basins, 42, 71–105.

677 Dick, H.J., and Bullen, T. (1984) Chromian spinel as a petrogenetic indicator in abyssal and
678 alpine-type peridotites and spatially associated lavas. Contributions to Mineralogy and
679 Petrology, 86, 54–76.

680 Dick, H.J., and Natland, J.H. (1996) Late-stage melt evolution and transport in the shallow
681 mantle beneath the East Pacific Rise. In Proceedings-Ocean Drilling Program Scientific
682 Results pp. 103–134. National Science Foundation.

683 Dick, H.J., Lissenberg, C.J., and Warren, J.M. (2010) Mantle melting, melt transport, and
684 delivery beneath a slow-spreading ridge: The paleo-MAR from 23 15′ N to 23 45′ N.
685 Journal of Petrology, 51, 425–467.

686 Dyar, M.D., McGuire, A.V., and Ziegler, R.D. (1989) Redox equilibria and crystal chemistry of
687 coexisting minerals from spinel lherzolite mantle xenoliths. American Mineralogist, 74,
688 969–980.

689 Fedortchouk, Y., Canil, D., and Carlson, J.A. (2005) Dissolution forms in Lac de Gras diamonds
690 and their relationship to the temperature and redox state of kimberlite magma.
691 Contributions to Mineralogy and Petrology, 150, 54–69.

692 Foley, S., Andronikov, A., Jacob, D., and Melzer, S. (2006) Evidence from Antarctic mantle
693 peridotite xenoliths for changes in mineralogy, geochemistry and geothermal gradients
694 beneath a developing rift. Geochimica et Cosmochimica Acta, 70, 3096–3120.

695 Frost, B.R. (1991) Introduction to oxygen fugacity and its petrologic importance. Reviews in
696 Mineralogy and Geochemistry, 25, 1–9.

697 Ghose, I., Cannat, M., and Seyler, M. (1996) Transform fault effect on mantle melting in the
698 MARK area (Mid-Atlantic Ridge south of the Kane transform). Geology, 24, 1139–1142.

699 Gudmundsson, G., and Wood, B. (1995) Experimental tests of garnet peridotite oxygen
700 barometry. Contributions to Mineralogy and Petrology, 119, 56–67.

701 Hamlyn, P.R., and Bonatti, E. (1980) Petrology of mantle-derived ultramafics from the Owen
702 Fracture Zone, northwest Indian Ocean: implications for the nature of the oceanic upper
703 mantle. Earth and Planetary Science Letters, 48, 65–79.

704 Hellebrand, E., and Snow, J.E. (2003) Deep melting and sodic metasomatism underneath the
705 highly oblique-spreading Lena Trough (Arctic Ocean). Earth and Planetary Science
706 Letters, 216, 283–299.

707 Hellebrand, E., Snow, J.E., Hoppe, P., and Hofmann, A.W. (2002a) Garnet-field melting and
708 late-stage refertilization in “residual”abyssal peridotites from the Central Indian Ridge.
709 Journal of Petrology, 43, 2305–2338.

710 Hellebrand, E., Snow, J.E., and Mühe, R. (2002b) Mantle melting beneath Gakkel Ridge (Arctic
711 Ocean): abyssal peridotite spinel compositions. Chemical Geology, 182, 227–235.

712 Herd, C.D. (2008) Basalts as probes of planetary interior redox state. Reviews in Mineralogy and
713 Geochemistry, 68, 527–553.

714 Ionov, D., and Wood, B. (1992) The oxidation state of subcontinental mantle: oxygen
715 thermobarometry of mantle xenoliths from central Asia. Contributions to Mineralogy and
716 Petrology, 111, 179–193.

717 Irvine, T. (1965) Chromian spinel as a petrogenetic indicator: Part 1. Theory. Canadian Journal
718 of Earth Sciences, 2, 648–672.

719 Jarosewich, E., Nelen, J., and Norberg, J.A. (1980) Reference Samples for Electron Microprobe
720 Analysis*. Geostandards Newsletter, 4, 43–47.

721 Jarosewich, E., Gooley, R., and Husler, J. (1987) Chromium Augite-A New Microprobe
722 Reference Sample. Geostandards Newsletter, 11, 197–198.

723 Jaroslow, G., Hirth, G., and Dick, H. (1996) Abyssal peridotite mylonites: implications for grain-
724 size sensitive flow and strain localization in the oceanic lithosphere. Tectonophysics, 256,
725 17–37.

726 Johnson, K., and Dick, H.J. (1992) Open system melting and temporal and spatial variation of
727 peridotite and basalt at the Atlantis II fracture zone. Journal of Geophysical Research:
728 Solid Earth, 97, 9219–9241.

729 Johnson, K., Dick, H.J., and Shimizu, N. (1990) Melting in the oceanic upper mantle: an ion
730 microprobe study of diopsides in abyssal peridotites. Journal of Geophysical Research:
731 Solid Earth, 95, 2661–2678.

732 Juteau, T., Berger, E., and Cannat, M. (1990) Serpentinized, residual mantle peridotites from the
733 MAR Median Valley, ODP hole 670A (21 10′ N, 45 02′ W, Leg 109): primary
734 mineralogy and geothermometry. In Proceedings of Ocean Drilling Program. Scientific
735 Results Vol. 106, p. 109.

736 Kelley, K.A., and Cottrell, E. (2012) The influence of magmatic differentiation on the oxidation
737 state of Fe in a basaltic arc magma. Earth and Planetary Science Letters, 329, 109–121.

738 Komor, S., Grove, T., and Hébert, R. (1990) Abyssal peridotites from ODP Hole 670A (21 10'N,
739 45 02'W): residues of mantle melting exposed by non-constructive axial divergence. In
740 Proceedings of Ocean Drilling Program, Scientific Results pp. 85–101.

741 Lassiter, J., Byerly, B., Snow, J., and Hellebrand, E. (2014) Constraints from Os-isotope
742 variations on the origin of Lena Trough abyssal peridotites and implications for the
743 composition and evolution of the depleted upper mantle. Earth and Planetary Science
744 Letters, 403, 178–187.

745 Li, J., Kornprobst, J., Vielzeuf, D., and Fabriès, J. (1995) An improved experimental calibration
746 of the olivine-spinel geothermometer. Chinese Journal of Geochemistry, 14, 68–77.

747 Li, Z.-X.A., and Lee, C.-T.A. (2004) The constancy of upper mantle fO 2 through time inferred
748 from V/Sc ratios in basalts. Earth and Planetary Science Letters, 228, 483–493.

749 Lucas, H., Muggeridge, M., and McConchie, D. (1988) Iron in kimberlitic ilmenites and
750 chromian spinels: a survey of analytical techniques. In Kimberlites and related rocks: 4th
751 Intern Kimberlite Conf Perth pp. 311–320.

752 Luhr, J.F., and Aranda-Gómez, J.J. (1997) Mexican peridotite xenoliths and tectonic terranes:
753 correlations among vent location, texture, temperature, pressure, and oxygen fugacity.
754 Journal of Petrology, 38, 1075–1112.

755 MacGregor, I.D. (2015) Empirical geothermometers and geothermobarometers for spinel
756 peridotite phase assemblages. International Geology Review, 57, 1940–1974.

757 Mallick, S., Dick, H.J., Sachi-Kocher, A., and Salters, V.J. (2014) Isotope and trace element
758 insights into heterogeneity of subridge mantle. Geochemistry, Geophysics, Geosystems,
759 15, 2438–2453.

760 Mattioli, G.S., and Wood, B.J. (1988) Magnetite activities across the MgAl2O4-Fe3O4 spinel
761 join, with application to thermobarometric estimates of upper mantle oxygen fugacity.
762 Contributions to Mineralogy and Petrology, 98, 148–162.

763 Michael, P., and Bonatti, E. (1985) Petrology of ultramafic rocks from site-556, site-558, and
764 site-560 in the North-Atlantic. Initial Reports of the Deep Sea Drilling Project, 82, 523–
765 528.

766 Morishita, T., Maeda, J., Miyashita, S., Kumagai, H., Matsumoto, T., and Dick, H.J. (2007)
767 Petrology of local concentration of chromian spinel in dunite from the slow-spreading
768 Southwest Indian Ridge. European Journal of Mineralogy, 19, 871–882.

769 Myers, J. t, and Eugster, H. (1983) The system Fe-Si-O: Oxygen buffer calibrations to 1,500 K.
770 Contributions to Mineralogy and Petrology, 82, 75–90.

771 Nasir, S., Everard, J., McClenaghan, M., Bombardieri, D., and Worthing, M. (2010) The
772 petrology of high pressure xenoliths and associated Cenozoic basalts from Northeastern
773 Tasmania. Lithos, 118, 35–49.

774 Niida, K. (1997) 12, Mineralogy of Mark peridotites: replacement through magma chaneling
775 examined from Hole 920D, Mark area. Proc. Ocean Dril. Prog, 153.

776 O'Neill, H.S. (1987) Quartz-fayalite-iron and quartz-fayalite-magnetite equilibria and the free
777 energy of formation of fayalite (Fe2SiO4) and magnetite (Fe3O4). American
778 Mineralogist, 72, 67–75.

779 O'Neill, H.S.C., and Wall, V. (1987) The Olivine—Orthopyroxene—Spinel oxygen
780 geobarometer, the nickel precipitation curve, and the oxygen fugacity of the Earth's
781 Upper Mantle. Journal of Petrology, 28, 1169–1191.

782 Parkinson, I.J., and Arculus, R.J. (1999) The redox state of subduction zones: insights from arc-
783 peridotites. Chemical Geology, 160, 409–423.

784 Parkinson, I.J., and Pearce, J.A. (1998) Peridotites from the Izu–Bonin–Mariana forearc (ODP
785 Leg 125): evidence for mantle melting and melt–mantle interaction in a supra-subduction
786 zone setting. Journal of Petrology, 39, 1577–1618.

787 Pouchou, J., and Pichoir, F. (1986) Very high elements X-ray microanalysis: recent models of
788 quantification. Journal de Microscopie et de Spectroscopie Electroniques, 11, 229–250.

789 Prinz, M., Keil, K., Green, J., Reid, A., Bonatti, E., and Honnorez, J. (1976) Ultramafic and
790 mafic dredge samples from the equatorial Mid-Atlantic ridge and fracture zones. Journal
791 of Geophysical Research, 81, 4087–4103.

792 Qi, Q., Taylor, L.A., and Zhou, X. (1995) Petrology and geochemistry of mantle peridotite
793 xenoliths from SE China. Journal of Petrology, 36, 55–79.

794 Robie, R.A., Hemingway, B.S., and Fisher, J.R. (1995) Thermodynamic properties of minerals
795 and related substances at 298.15 K and 1 bar (10^ 5 Pascals) pressure and at higher
796 temperatures. USGPO; For sale by US Geological Survey, Information Services,.

797 Ross, K., and Elthon, D. (1997) Extreme incompatible trace-element depletion of diopside in
798 residual mantle from south of the Kane fracture zone. In Proc. ODP, Sci. Results Vol.
799 153.

800 Sack, R.O., and Ghiorso, M.S. (1991a) An internally consistent model for the thermodynamic
801 properties of Fe- Mg-titanomagnetite-aluminate spinels. Contributions to Mineralogy and
802 Petrology, 106, 474–505.

803 ——— (1991b) Chromian spinels as petrogenetic indicators; thermodynamics and petrological
804 applications. American Mineralogist, 76, 827–847.

805 Seyler, M., Cannat, M., and Mevel, C. (2003) Evidence for major-element heterogeneity in the
806 mantle source of abyssal peridotites from the Southwest Indian Ridge (52 to 68 E).
807 Geochemistry, Geophysics, Geosystems, 4.

808 Seyler, M., Lorand, J.-P., Dick, H.J., and Drouin, M. (2007) Pervasive melt percolation reactions
809 in ultra-depleted refractory harzburgites at the Mid-Atlantic Ridge, 15 20′ N: ODP Hole
810 1274A. Contributions to Mineralogy and Petrology, 153, 303–319.

811 Shervais, J.W. (1982) Ti-V plots and the petrogenesis of modern and ophiolitic lavas. Earth and
812 planetary science letters, 59, 101–118.

813 Shibata, T., and Thompson, G. (1986) Peridotites from the Mid-Atlantic Ridge at 43 N and their
814 petrogenetic relation to abyssal tholeiites. Contributions to Mineralogy and Petrology, 93,
815 144–159.

816 Smith, J., and Ribbe, P. (1966) X-ray-emission microanalysis of rock-forming minerals III.
817 Alkali feldspars. The Journal of Geology, 197–216.

818 Snow, J.E. (1993) The isotope geochemistry of abyssal peridotites and related rocks(Ph. D.
819 Thesis- MIT).

820 Stephens, C. (1997) Heterogeneity of oceanic peridotite from the western canyon wall at MARK:
821 results from site 920. In Proceedings of the Ocean Drilling Program. Scientific Results
822 Vol. 153, pp. 285–303. Ocean Drilling Program.

823 Stormer, J.C. (1983) The effects of recalculation on estimates of temperature and oxygen
824 fugacity from analyses of multicomponent iron-titanium oxides. American Mineralogist,
825 68, 586–594.

826 Wang, J., Hattori, K.H., Kilian, R., and Stern, C.R. (2007) Metasomatism of sub-arc mantle
827 peridotites below southernmost South America: reduction of fO2 by slab-melt.
828 Contributions to Mineralogy and Petrology, 153, 607–624.

829 Wang, J., Hattori, K.H., Li, J., and Stern, C.R. (2008) Oxidation state of Paleozoic
830 subcontinental lithospheric mantle below the Pali Aike volcanic field in southernmost
831 Patagonia. Lithos, 105, 98–110.

832 Wang, J., Hattori, K., Xu, W., Yang, Y., Xie, Z., Liu, J., and Song, Y. (2012) Origin of
833 ultramafic xenoliths in high-Mg diorites from east-central China based on their oxidation
834 state and abundance of platinum group elements. International Geology Review, 54,
835 1203–1218.

836 Warren, J. (2016) Global Variations in Abyssal Peridotite Compositions. Lithos.

837 Warren, J.M., and Shimizu, N. (2010) Cryptic variations in abyssal peridotite compositions:
838 evidence for shallow-level melt infiltration in the oceanic lithosphere. Journal of
839 Petrology, 51, 395–423.

840 Warren, J.M., Shimizu, N., Sakaguchi, C., Dick, H.J., and Nakamura, E. (2009) An assessment
841 of upper mantle heterogeneity based on abyssal peridotite isotopic compositions. Journal
842 of Geophysical Research: Solid Earth, 114.

843 Wood, B.J. (1990) An experimental test of the spinel peridotite oxygen barometer. Journal of
844 Geophysical Research: Solid Earth, 95, 15845–15851.

845 ——— (1991) Oxygen barometry of spinel peridotites. Reviews in Mineralogy and
846 Geochemistry, 25, 417–432.

847 Wood, B.J., and Banno, S. (1973) Garnet-orthopyroxene and orthopyroxene-clinopyroxene
848 relationships in simple and complex systems. Contributions to mineralogy and petrology,
849 42, 109–124.

850 Wood, B.J., and Nicholls, J. (1978) The thermodynamic properties of reciprocal solid solutions.
851 Contributions to Mineralogy and Petrology, 66, 389–400.

852 Wood, B.J., and Virgo, D. (1989) Upper mantle oxidation state: Ferric iron contents of lherzolite
853 spinels by 57Fe Mössbauer spectroscopy and resultant oxygen fugacities. Geochimica et
854 Cosmochimica Acta, 53, 1277–1291.

855 Wood, B.J., Bryndzia, L.T., and Johnson, K.E. (1990) Mantle oxidation state and its relationship
856 to tectonic environment and fluid speciation. Science, 248, 337–345.

857 Woodland, A.B., Kornprobst, J., and Wood, B.J. (1992) Oxygen thermobarometry of orogenic
858 lherzolite massifs. Journal of Petrology, 33, 203–230.

859 Workman, R.K., and Hart, S.R. (2005) Major and trace element composition of the depleted
860 MORB mantle (DMM). Earth and Planetary Science Letters, 231, 53–72.

861 Wright, D.J., Bloomer, S.H., MacLeod, C.J., Taylor, B., and Goodlife, A.M. (2000) Bathymetry
862 of the Tonga Trench and Forearc: a map series. Marine Geophysical Researches, 21,
863 489–512.

Zhou, H., and Dick, H.J. (2013) Thin crust as evidence for depleted mantle supporting the Marion Rise. Nature, 494, 195–200.

Figure Captions

Figure 1: Uncorrected electron microprobe analyses of Wood spinels from Sessions S1-S3. Sample-average uncorrected $Fe^{3+}/\Sigma Fe$ ratios determined by EPMA in sessions S1-S3 (Table 2) plotted against $Fe^{3+}/\Sigma Fe$ ratios determined by Mössbauer spectroscopy. Vertical bars show the range of compositions for a given sample across all grains measured (Supplementary Table S1), indicating the degree of intergranular heterogeneity exhibited by a sample. Circles represent samples chosen for the correction set, and triangles represent samples chosen for the validation set. All other Wood spinels are represented with diamonds.

Figure 2: Compositional range of spinels included in the correction and validation sets. $Fe^{3+}/\Sigma Fe$ ratios by Mössbauer are from Wood and Virgo (1989), Bryndzia and Wood (1990), and Ionov and Wood (1992). MgO and Cr# of the correction set and validation set are EPMA measurements from this study (Table 2), while values for the correction standards used by Wood and Virgo (1989) are as reported in that study. The correction set used in this study spans a similar range of Cr# and MgO (b) as the correction standards used by Wood and Virgo (1989), and $Fe^{3+}/\Sigma Fe$ ratios span a larger range (a). Taking all of these data together, $Fe^{3+}/\Sigma Fe$ ratio is not correlated with Cr# ($r^2 = 0.003$) or MgO (not shown, $r^2 < 0.001$), and MgO and Cr# are highly correlated ($r^2 = 0.93$).

Figure 3: Examples of the W&V89 correction applied to spinels from several independent analytical sessions. The first column (a, c, and e) shows uncorrected $Fe^{3+}/\Sigma Fe$ ratios by EPMA of the correction set spinels measured at the start of each session and at the end of each session,

886 along with validation set spinels analyzed in between. These are plotted against their published
887 $Fe^{3+}/\Sigma Fe$ ratios measured by Mössbauer. The second column (b, d, and f) shows the same
888 measurements after correction of the EPMA data using the Wood and Virgo (1989) method.
889 Uncorrected EPMA analyses from session A1 plot around the 1:1 line (a), and the W&V89
890 correction causes only imperceptible changes to the corrected $Fe^{3+}/\Sigma Fe$ ratios (b). Uncorrected
891 EPMA analyses from session B3 (c,d) are offset from the 1:1 line and display a relatively high
892 degree of scatter around the trend with Mössbauer data (c). The W&V89 correction decreases
893 scatter in the data and shifts it upward so that the corrected data lie on the 1:1 line (d).
894 Uncorrected EPMA analyses from session B4 (e,f) are offset from the 1:1 line but are relatively
895 tightly clustered along a linear trend with the Mössbauer data (e). The W&V89 correction shifts
896 $Fe^{3+}/\Sigma Fe$ ratios onto the 1:1 line (f).

897 **Figure 4: Relationship between Cr# and $\Delta Fe^{3+}/\Sigma Fe^{Möss\text{-}EPMA}$ in uncorrected analyses of the**
898 **correction set spinels.** Cr# and $\Delta Fe^{3+}/\Sigma Fe^{Möss\text{-}EPMA}$ are the measured parameters that contribute
899 directly to the W&V89 correction and the same analytical sessions are shown as in Figure 3. In
900 Session A1 (a), Cr# and $\Delta Fe^{3+}/\Sigma Fe^{Möss\text{-}EPMA}$ are uncorrelated ($r^2 = 0.01$) and $\Delta Fe^{3+}/\Sigma Fe^{Möss\text{-}EPMA}$
901 is near zero, so the W&V89 correction makes negligible adjustments to the $Fe^{3+}/\Sigma Fe$ ratio, as
902 expected given that the uncorrected data already overlapped the Mössbauer values. In Session B3
903 (b), Cr# and $\Delta Fe^{3+}/\Sigma Fe^{Möss\text{-}EPMA}$ are correlated (r^2=0.81), with slope and intercept both
904 significantly different from zero. The W&V89 correction shifts $Fe^{3+}/\Sigma Fe$ ratios of all samples
905 upward and Cr-poor spinels are adjusted more than Cr-rich spinels. In Session B4 (c), Cr# and
906 $\Delta Fe^{3+}/\Sigma Fe^{Möss\text{-}EPMA}$ are poorly correlated (r^2=0.10) with slope near zero but an intercept
907 significantly different from zero; consequently, the W&V89 correction shifts all $Fe^{3+}/\Sigma Fe$ ratios
908 upward by a nearly constant correction factor.

Figure 5: Literature compilation of spinel $Fe^{3+}/\Sigma Fe$ ratios measured by Mössbauer spectroscopy and calculated from EPMA. Uncorrected spinel $Fe^{3+}/\Sigma Fe$ ratios calculated from EPMA analyses of natural peridotite - and basalt-hosted spinels plotted against $Fe^{3+}/\Sigma Fe$ ratios of the same spinels analyzed by Mössbauer spectroscopy (a). Uncorrected spinel $Fe^{3+}/\Sigma Fe$ ratios by EPMA are biased to low $Fe^{3+}/\Sigma Fe$, with a mean $\Delta Fe^{3+}/\Sigma Fe^{Möss\text{-}EPMA}$ of 0.022±0.049 (1σ). After correction by the W&V89 method, $Fe^{3+}/\Sigma Fe$ ratios deviate less from the 1:1 line and are more evenly distributed around it (b), with a mean $\Delta Fe^{3+}/\Sigma Fe^{Möss\text{-}EPMA}$ of -0.007±0.021 (1σ).

Figure 6: Mean $Fe^{3+}/\Sigma Fe$ ratios of the validation set spinels measured by Mössbauer spectroscopy and calculated from EPMA. Mean uncorrected (a) and corrected (b) $Fe^{3+}/\Sigma Fe$ ratios by EPMA (Table 4) were calculated by taking the unweighted average of the mean $Fe^{3+}/\Sigma Fe$ ratios of all analytical sessions (A1-A4 and B1-B4; Supplementary Table S2). Error bars are two standard deviations.

Figure 7: Relationship between analytical precision of spinel $Fe^{3+}/\Sigma Fe$ ratios and total concentration of Fe for spinels from the validation set, Hawaiian xenoliths and Tonga. Magnitude of 1 standard deviation in corrected $Fe^{3+}/\Sigma Fe$ ratios measured across all sessions (A1-A4 and B1-B4, Supplementary Table S2) for validation set and Hawaiian spinels as a function of the inverse of the multi-session average total Fe concentration on a 3 cation basis (a). In black is the best fit line through the origin ($r^2 = 0.57$). Tonga sample BMRG08-98-2-2 was not included in this fit because it does not plot near the global trend in Cr#-MgO (Figure 8). The equation for this line is given in the text (eq. 3), and we use it to calculate precision in our corrected measurements of $Fe^{3+}/\Sigma Fe$ ratios of unknown spinel samples. Deviations of each session average (Supplementary Table S2) from their respective multisession means (Table 4) plotted as a

function of total Fe concentration on a 3 cation basis (b). The 1σ error envelope is calculated using eq. 3.

Figure 8: Relationship between MgO concentration and Cr# of natural peridotite spinels. Samples are separated by tectonic setting: abyssal peridotites (n = 743) from the compilation of Warren (2016): (Prinz et al. 1976; Hamlyn and Bonatti 1980; Dick and Bullen 1984; Michael and Bonatti 1985; Shibata and Thompson 1986; Dick 1989; Bryndzia and Wood 1990; Johnson et al. 1990; Juteau et al. 1990; Komor et al. 1990; Bonatti et al. 1992, 1993; Cannat et al. 1992; Johnson and Dick 1992; Snow 1993; Constantin et al. 1995; Arai and Matsukage 1996; Dick and Natland 1996; Ghose et al. 1996; Jaroslow et al. 1996; Niida 1997; Ross and Elthon 1997; Stephens 1997; Hellebrand et al. 2002a, 2002b; Brunelli et al. 2003; Hellebrand and Snow 2003; Seyler et al. 2003, 2007; Coogan et al. 2004; Workman and Hart 2005; Morishita et al. 2007; Cipriani et al. 2009; Warren et al. 2009; Brunelli and Seyler 2010; Dick et al. 2010; Warren and Shimizu 2010; Zhou and Dick 2013; Lassiter et al. 2014; Mallick et al. 2014; D'Errico et al. 2016), continental xenoliths not associated with subduction (n = 154): (Wood and Virgo 1989; Ionov and Wood 1992; Woodland et al. 1992), and supra-subduction zone for xenoliths and seafloor drilled samples from subduction-related settings (n = 85): (Wood and Virgo 1989; Canil et al. 1990; Luhr and Aranda-Gómez 1997; Parkinson and Pearce 1998). MgO and Cr# are correlated in the global data set (solid line, r^2=0.82, slope = -15.0±0.2, intercept = 21.46±0.07, 1σ). The slope defined by the correction set used in this study (dashed line, r^2=0.94, n = 7, slope = -11.6±1.4, intercept = 21.5±0.4, 1σ) is shallower, as is the line defined by the Wood spinels (not shown, r^2=0.92, n = 32, slope = -12.7±0.7, intercept = 21.80±0.17, 1σ). Also shown are Hawaiian xenoliths and Tonga peridotite BMRG08-98-2-2 from this study.

Figure 9: Effect of activity of magnetite in spinel on the calculation of relative f_{O2}. Calculated logf_{O2} relative to the quartz-fayalite-magnetite buffer (ΔQFM, Frost 1991 calibration) using all input parameters from sample 114923-57 at 1038 °C and 1.5 GPa and varying the value of $\log a_{Fe_3O_4}^{spl}$ while holding $Mg\#^{ol}$ and $(X_{Fe}^{M1} \cdot X_{Fe}^{M2})^{opx}$ constant (a). The dashed lines show ±1σ error on the corrected EMP measurement of spinel $Fe^{3+}/\Sigma Fe$ ratio calculated using eq. 3. Dotted lines show ±1σ error on the uncorrected EMP measurement of spinel $Fe^{3+}/\Sigma Fe$ ratio assuming a twofold increase in uncertainty for uncorrected measurements (see text). The increased uncertainty in f_{O2} at low activities of magnetite has been demonstrated previously by Ballhaus et al. (1991) and Parkinson and Arculus (1999). The dependence of logf_{O2} (ΔQFM) on $Fe^{3+}/\Sigma Fe$ ratio rather than activity of magnetite (b).

Figure 10: Relative f_{O2} and activity of magnetite in each of the four Hawaiian xenoliths and comparison between Wood (1991) and Ballhaus et al. (1991) formulations of the spinel-olivine-orthopyroxene oxybarometer. Log f_{O2} (ΔQFM; a) and $\log a_{Fe_3O_4}^{spl}$ (b), calculated from corrected $Fe^{3+}/\Sigma Fe$ ratios, for each session in which a given spinel was analyzed (Supplementary Table S4). The olivine and orthopyroxene compositions in Table 3 were used for all f_{O2} calculations. Uncertainty in log f_{O2} (ΔQFM) includes contributions from analytical uncertainty on each phase (a). Uncertainty in $\log a_{Fe_3O_4}^{spl}$ was determined as described in the Supplementary material. Uncertainty in corrected $Fe^{3+}/\Sigma Fe$ ratios was calculated using eq. 3. f_{O2} relative to the QFM buffer (Frost 1991), calculated for each measurement of the four Hawaiian spinel lherzolite xenoliths (c). Relative f_{O2} on the x-axis was calculated using the Eq. 4 and the MELTS Supplemental Calculator (Sack and Ghiorso 1991a, 1991b) to calculate $a_{Fe_3O_4}^{spl}$. Relative f_{O2} on the y-axis was calculated following the methodology of Ballhaus et al. (1991). Error using the

975 Ballhaus et al. (1991) method was estimated by propagating through the Ballhaus et al. (1991)

976 oxybarometer our estimates of uncertainty in spinel $Fe^{3+}/\Sigma Fe$ ratio and olivine Mg#.

977

Table 1. Elements, detector crystals, count times, and primary standards used in EPMA analysis

element	detector crystal	peak count time (s)	background time (s)	primary standard (Smithsonian catalog number)
spinel analysis				
Si	TAP	30	15	San Carlos olivine (NMNH 111312 44)
Ti	PETJ	40	20	Kakanui hornblende (NMNH 143965)
Al	TAP	40	20	Spinel[a] (NMNH 136804)
Cr	LiFH	30	15	Tiebaghi Mine chromite (NMNH 117075)
Fe	LiFH	30	15	San Carlos olivine
Mn	LiF	30	15	Manganite[a] (NMNH 157972)
Mg	TAP	30	15	San Carlos olivine
Ca	PETJ	30	15	Wollastonite[a] (synthetic, F.R. Boyd, no catalog #)
Na	TAP	30	15	Kakanui hornblende
Ni	LiF	40	20	San Carlos olivine
olivine and orthopyroxene analysis				
Si	TAP	20	10	olivine – S.C. olivine, orthopyroxene - Johnstown Meteorite hypersthene (USNM 746)
Ti	PETJ	20	10	Kakanui hornblende
Al	TAP	20	10	Spinel[a]
Cr	LiFH	20	10	Tiebaghi Mine chromite
Fe	LiFH	20	10	San Carlos olivine
Mn	LiF	20	10	Manganite[a]
Mg	TAP	20	10	San Carlos olivine
Ca	PETJ	20	10	Wollastonite[a]
Na	TAP	20	10	Roberts Victor Mine omphacite (NMNH 110607)
K	PETJ	20	10	Asbestos microcline[b] (NMNH 143966)
Ni	LiF	20	10	San Carlos olivine

All standards from Jarosewich et al. (1980), except as follows:

[a]Smithsonian internal reference standard (compositions given in Supplemental Table S5)

[b]Smith and Ribbe (1966)

978

979

Table 2. Sample average[a] uncorrected compositions of all Wood spinels by electron microprobe analysis

Analytical Session S1 (08 Nov 13)								*Analytical Session S2 (21 Nov 13)*		
Sample name	IO5657[b]	PS211[c]	IO5818	IO5650[c]	OC231350[c]	PS212[c]	PS216	MHP79-4	MO4230-16	Vi314-58[c]
n[d]	5	5	4	5	5	4	5	18	15	18
SiO_2	n.d.	n.d.	n.d.	n.d.	n.d.	n.d.	n.d.	n.d.	n.d.	n.d.
TiO_2	0.042(6)	0.072(14)	0.037(10)	0.046(25)	0.061(15)	0.025(5)	0.097(10)	0.100(9)	0.08(6)	0.071(11)
Al_2O_3	54.1(3)	32.2(12)	52.2(29)	54.8(6)	51.3(19)	36.3(5)	31.7(29)	58.91(16)	59.7(4)	59.2(2)
Cr_2O_3	14.25(8)	35.6(13)	15.2(20)	13.3(4)	16.5(19)	32.5(5)	37.0(31)	9.64(17)	7.94(17)	8.47(15)
FeO*	10.9(2)	15.3(5)	11.7(11)	10.7(3)	11.8(2)	13.5(2)	14.5(8)	9.77(7)	11.3(3)	10.98(6)
MnO	0.113(6)	0.187(7)	0.116(22)	0.111(20)	0.110(11)	0.171(15)	0.21(3)	0.099(18)	0.104(12)	0.106(18)
MgO	19.4(3)	15.36(18)	19.2(7)	19.74(12)	19.15(16)	16.4(3)	15.4(6)	21.06(19)	20.4(2)	20.62(16)
CaO	n.d.	n.d.	n.d.	n.d.	n.d.	n.d.	n.d.	0.014(10)	0.015(12)	0.012(10)
Na_2O	n.d.	n.d.	n.d.	n.d.	n.d.	n.d.	n.d.	n.d.	n.d.	n.d.
NiO	0.28(4)	0.140(19)	0.30(3)	0.293(17)	0.294(14)	0.15(3)	0.10(2)	0.375(17)	0.387(17)	0.385(18)
Total	99.1	98.8	98.9	99.0	99.2	98.9	99.0	99.96	99.9	99.9
Cr#	0.150(1)	0.426(13)	0.164(20)	0.140(4)	0.177(18)	0.375(4)	0.439(30)	0.099(2)	0.082(2)	0.087(1)
$Fe^{3+}/\Sigma Fe$ (EMP, this study)	0.067(24)	0.152(9)	0.13(7)	0.09(3)	0.131(28)	0.107(10)	0.107(16)	0.109(26)	0.135(25)	0.147(15)
$Fe^{3+}/\Sigma Fe$ (Moss.)[e]	0.058	0.131	0.089	0.054	0.094	0.092	0.083	0.13	0.15	0.14
$Fe^{3+}/\Sigma Fe$ (EMP)[e]	0.048	0.140	0.077	0.073	0.093	0.095	0.067	0.13	0.14	0.15

980

981

Table 2 continued.

Analytical Session S2 (21 Nov 13)											
Sample name	MO4334-14[b]	BAR8603-2	BAR8601-9	KLB8320[b]	BAR8601-10[b]	MHP1	MO4334-2	IM8703[b]	DAR8529-6	DB8803-3[b]	SC8804
n	15	15	15	15	15	15	15	15	15	15	15
SiO_2	n.d.	n.d.	n.d.	n.d.	n.d.	n.d.	n.d.	n.d.	n.d.	n.d.	n.d.
TiO_2	0.145(9)	0.098(18)	0.088(12)	0.127(12)	0.174(11)	0.169(8)	0.10(3)	0.065(18)	0.057(8)	0.10(3)	0.429(13)
Al_2O_3	63.2(4)	57.4(4)	55.0(3)	57.5(6)	38.66(13)	58.86(15)	59.4(16)	50.2(19)	56.1(4)	22.7(3)	45.6(4)
Cr_2O_3	4.3(3)	10.0(4)	12.8(2)	9.4(5)	29.61(20)	8.578(7)	8.0(15)	14.4(18)	11.1(4)	45.0(4)	20.6(3)
FeO*	10.46(10)	10.94(12)	10.78(7)	11.56(15)	12.48(10)	10.53(7)	10.59(20)	15.4(8)	12.02(10)	15.85(22)	14.4(3)
MnO	0.084(11)	0.099(11)	0.107(11)	0.111(20)	0.154(15)	0.107(18)	0.097(16)	0.141(21)	0.112(19)	0.223(21)	0.157(13)
MgO	21.4(2)	20.65(11)	20.75(13)	20.78(19)	18.09(11)	21.06(10)	21.0(2)	18.7(5)	20.13(19)	14.84(17)	18.0(3)
CaO	n.d.	0.014(10)	0.014(9)	0.014(10)	0.011(7)	n.d.	0.014(11)	0.023(9)	0.017(8)	0.022(14)	0.023(10)
Na_2O	n.d.	n.d.	n.d.	n.d.	n.d.	n.d.	n.d.	n.d.	n.d.	n.d.	n.d.
NiO	0.519(26)	0.367(24)	0.354(18)	0.355(21)	0.245(21)	0.38(3)	0.41(3)	0.37(3)	0.38(2)	0.143(16)	0.266(17)
Total	100.2	99.6	99.9	99.8	99.42	99.68	99.6	99.3	100.0	99.0	99.4
Cr#	0.044(3)	0.105(3)	0.135(2)	0.098(5)	0.339(2)	0.0890(7)	0.083(14)	0.162(18)	0.117(4)	0.571(4)	0.233(3)
$Fe^{3+}/\Sigma Fe$ (EMP, this study)	0.157(23)	0.176(14)	0.199(18)	0.229(22)	0.191(15)	0.173(17)	0.177(19)	0.305(19)	0.201(12)	0.222(7)	0.200(17)
$Fe^{3+}/\Sigma Fe$ (Moss.)[e]	0.16	0.16	0.18	0.22	0.18	0.16	0.17	0.32	0.19	0.2	0.22
$Fe^{3+}/\Sigma Fe$ (EMP)[e]	0.15	0.15	0.19	0.23	0.18	0.17	0.16	0.31	0.19	0.21	0.22

982

983

Table 2 continued.

Analytical Session S2 (21 Nov 13)			*Analytical Session S3 (02 Jan 14)*								
Sample name	BAR8601-26	MBR8305	IM8702	MO4334-11	Vi313-37	Vi314-5[b]	KLB8311	KLB8304[c]	Vi314-56	DAR8505-1	DB8803-1
n	15	16	18	10	15	10	5	10	10	10	10
SiO_2	0.035(13)	n.d.	n.d.	n.d.	n.d.	n.d.	n.d.	n.d.	n.d.	n.d.	n.d.
TiO_2	0.455(22)	0.119(10)	0.06(3)	0.262(13)	0.37(3)	0.495(15)	0.109(11)	0.100(8)	0.117(9)	0.099(17)	0.161(16)
Al_2O_3	58.7(3)	54.7(3)	50.6(19)	57.7(12)	44.1(12)	44.7(3)	25.76(13)	61.2(4)	59.9(4)	51.8(4)	30.1(4)
Cr_2O_3	6.9(4)	12.34(14)	16.1(19)	9.7(12)	23.1(11)	20.80(15)	43.85(16)	6.24(12)	8.02(14)	15.5(4)	39.1(5)
FeO*	11.92(24)	11.32(12)	12.4(4)	11.0(3)	13.02(22)	14.96(14)	13.58(6)	11.03(8)	10.90(7)	12.2(7)	13.23(15)
MnO	0.101(14)	0.101(16)	0.116(19)	0.099(13)	0.134(15)	0.126(8)	0.188(12)	0.099(11)	0.109(13)	0.120(20)	0.188(21)
MgO	21.13(14)	20.91(21)	19.6(4)	20.88(21)	18.83(21)	18.35(8)	16.22(8)	21.29(13)	20.60(15)	19.86(17)	16.66(15)
CaO	0.017(14)	0.019(12)	0.019(6)	0.013(8)	0.017(12)	n.d.	n.d.	n.d.	n.d.	n.d.	n.d.
Na_2O	n.d.	n.d.	n.d.	n.d.	n.d.	n.d.	n.d.	n.d.	n.d.	n.d.	n.d.
NiO	0.349(23)	0.376(18)	0.32(3)	0.36(3)	0.301(20)	0.29(3)	0.148(19)	0.34(3)	0.382(20)	0.317(19)	0.165(13)
Total	99.6	99.8	99.2	100.0	99.9	99.8	99.86	100.3	100.0	99.9	99.6
Cr#	0.073(4)	0.132(1)	0.176(18)	0.101(11)	0.260(10)	0.238(2)	0.533(2)	0.064(1)	0.082(1)	0.167(4)	0.466(5)
$Fe^{3+}/\Sigma Fe$ (EMP, this study)	0.251(16)	0.270(22)	0.236(22)	0.181(11)	0.221(10)	0.256(9)	0.189(10)	0.194(12)	0.123(17)	0.22(3)	0.167(15)
$Fe^{3+}/\Sigma Fe$ (Moss.)[e]	0.24	0.27	0.26	0.24	0.25	0.27	0.21	0.22	0.13	0.23	0.25
$Fe^{3+}/\Sigma Fe$ (EMP)[e]	0.24	0.26	0.26	0.25	0.24				0.13	0.26	

[a]grain averages can be found in the appendix

[b]selected for the correction set

[c]selected for the validation set

[d]n is the total number of analyses from all grains

[e]measurements reported by Wood and Virgo (1989), Bryndzia and Wood (1990), or Ionov and Wood (1992)

984

985

Table 3. Compositions of Hawaiian xenolith olivine and orthopyroxene by EMP

sample	68-551-20		69-SAL-41		69-SAL-56		69-SAL-57	
NMNH catalog no.	114885-3		114923-41		114923-56		114923-57	
phase	olivine	orthopyroxene	olivine	orthopyroxene	olivine	orthopyroxene	olivine	orthopyroxene
n	10	10	10	10	8	9	10	10
SiO_2	40.6(4)	55.40(28)	40.3(4)	54.5(5)	40.03(24)	54.0(4)	40.74(29)	55.6(4)
TiO_2	n.d.	0.025(11)	n.d.	0.112(14)	n.d.	0.160(14)	n.d.	0.056(19)
Al_2O_3	n.d.	2.66(11)	n.d.	4.77(18)	n.d.	5.3(4)	n.d.	3.31(14)
Cr_2O_3	n.d.	0.74(5)	n.d.	0.42(4)	0.013(12)	0.41(6)	n.d.	0.66(4)
FeO*	8.89(7)	5.70(7)	9.75(5)	6.20(5)	10.12(6)	6.499(17)	8.53(4)	5.50(4)
MnO	0.136(19)	0.141(15)	0.149(15)	0.148(23)	0.134(12)	0.162(29)	0.131(18)	0.149(16)
MgO	50.0(3)	33.07(25)	49.38(20)	32.66(25)	48.78(24)	31.95(5)	50.9(4)	34.01(18)
CaO	0.033(8)	2.0(4)	0.040(5)	0.70(9)	0.059(8)	0.85(18)	0.042(9)	0.73(6)
Na_2O	n.d.	n.d.	n.d.	0.135(22)	n.d.	0.133(18)	n.d.	0.088(10)
K_2O	n.d.	n.d.	n.d.	n.d.	n.d.	n.d.	n.d.	n.d.
NiO	0.39(4)	0.103(25)	0.360(27)	0.096(14)	0.35(4)	0.107(29)	0.39(3)	0.082(23)
Total	100.0	100.0	99.9	99.7	99.49	99.5	100.7	100.2

986

987

988

Table 4. Multi-session average compositions[a] of validation set, Hawaiian, and Tongan spinels

	Validation Set						
sample name	PS211	PS212	OC231350	KLB8304	MBR8313	Vi314-58	IO5650
n	75	76	36	66	70	67	31
SiO_2	n.d.	n.d.	n.d.	n.d.	n.d.	n.d.	n.d.
TiO_2	0.070(4)	0.022(3)	0.067(10)	0.103(5)	0.213(11)	0.076(3)	0.051(8)
Al_2O_3	32.8(8)	37.4(10)	50.9(16)	60.7(12)	49.1(10)	59.2(12)	56.3(12)
Cr_2O_3	35.8(4)	32.0(4)	17.1(6)	6.17(6)	17.13(16)	8.54(6)	13.35(11)
FeO*	15.0(4)	13.16(23)	11.57(21)	11.09(14)	12.88(15)	10.84(11)	10.7(3)
MnO	0.190(7)	0.170(8)	0.122(5)	0.101(8)	0.126(7)	0.108(6)	0.111(10)
MgO	15.28(19)	16.28(11)	18.78(17)	21.05(27)	19.33(21)	20.41(19)	19.51(20)
CaO	0.002(2)	0.002(2)	n.d.	n.d.	0.019(7)	0.010(5)	n.d.
Na_2O	n.d.	n.d.	n.d.	n.d.	n.d.	n.d.	n.d.
NiO	0.145(5)	0.157(7)	0.283(12)	0.357(13)	0.345(7)	0.381(11)	0.305(14)
Total	99.1	99.1	98.7	99.6	99.1	99.5	100.2
Cr#	0.423(6)	0.365(7)	0.184(7)	0.064(1)	0.190(4)	0.088(2)	0.137(3)
$Fe^{3+}/\Sigma Fe$ (EPMA, corrected)	0.133(12)	0.079(15)	0.12(2)	0.24(3)	0.28(2)	0.16(2)	0.04(3)
$Fe^{3+}/\Sigma Fe$ (EPMA, uncorrected)	0.111(31)	0.054(29)	0.08(5)	0.19(6)	0.25(5)	0.12(6)	0.00(7)
$Fe^{3+}/\Sigma Fe$ (Möss.)[b]	0.131	0.092	0.094	0.22	0.29	0.14	0.054

989

Table 4 continued.

	Hawaiian Xenoliths				Tonga Peridotite
	68-551-20	69-SAL-41	69-SAL-56	69-SAL-57	BMRG08-98-2-2
sample name	114885-3	114923-41	114923-56	114923-57	
n	30	74	75	39	37
SiO_2	n.d.	n.d.	n.d.	n.d.	n.d.
TiO_2	0.040(3)	0.093(3)	0.194(4)	0.266(4)	0.045(4)
Al_2O_3	32.0(10)	55.7(10)	57.1(11)	38.3(12)	16.33(19)
Cr_2O_3	35.2(5)	11.55(12)	9.00(9)	28.30(12)	50.9(9)
FeO*	16.83(15)	11.16(14)	11.87(13)	14.78(6)	21.6(7)
MnO	0.202(14)	0.114(6)	0.110(6)	0.163(4)	0.353(18)
MgO	14.4(4)	20.2(4)	20.5(3)	17.5(4)	9.1(4)
CaO	0.011(1)	n.d.	0.003(2)	n.d.	n.d.
Na_2O	n.d.	n.d.	n.d.	n.d.	n.d.
NiO	0.144(5)	0.348(10)	0.392(10)	0.253(8)	0.048(2)
Total	98.7	99.1	99.0	99.5	98.3
Cr#	0.424(8)	0.122(2)	0.096(2)	0.332(7)	0.676(4)
$Fe^{3+}/\Sigma Fe$ (EPMA, corrected)	0.172(18)	0.204(20)	0.270(23)	0.283(20)	0.086(15)
$Fe^{3+}/\Sigma Fe$ (EPMA, uncorrected)	0.149(34)	0.163(62)	0.227(62)	0.253(57)	0.081(14)
T (°C)[d]	902 (25)	1118(56)	1196(82)	1038(40)	
activity of magnetite[e]	0.0114	0.0100	0.0160	0.0183	
$\log f_{O2}(\Delta QFM)$[f]	$0.24^{+0.28}_{-0.29}$	$0.15^{+0.34}_{-0.37}$	$0.56^{+0.27}_{-0.29}$	$0.98^{+0.24}_{-0.25}$	

[a]complete analyses can be found in Supplementary Table S1

[b]measurements from Wood and Virgo (1989), Bryndzia and Wood (1990), or Ionov and Wood (1992)

[c]For Hawaiian samples, the sample number assigned by E.D. Jackson is given first then the NMNH collection number

[d]Li et al. (1995)

[e]MELTS Supplemental Calculator

[f]P = 1.5 GPa, QFM formulation of Frost (1991)

990

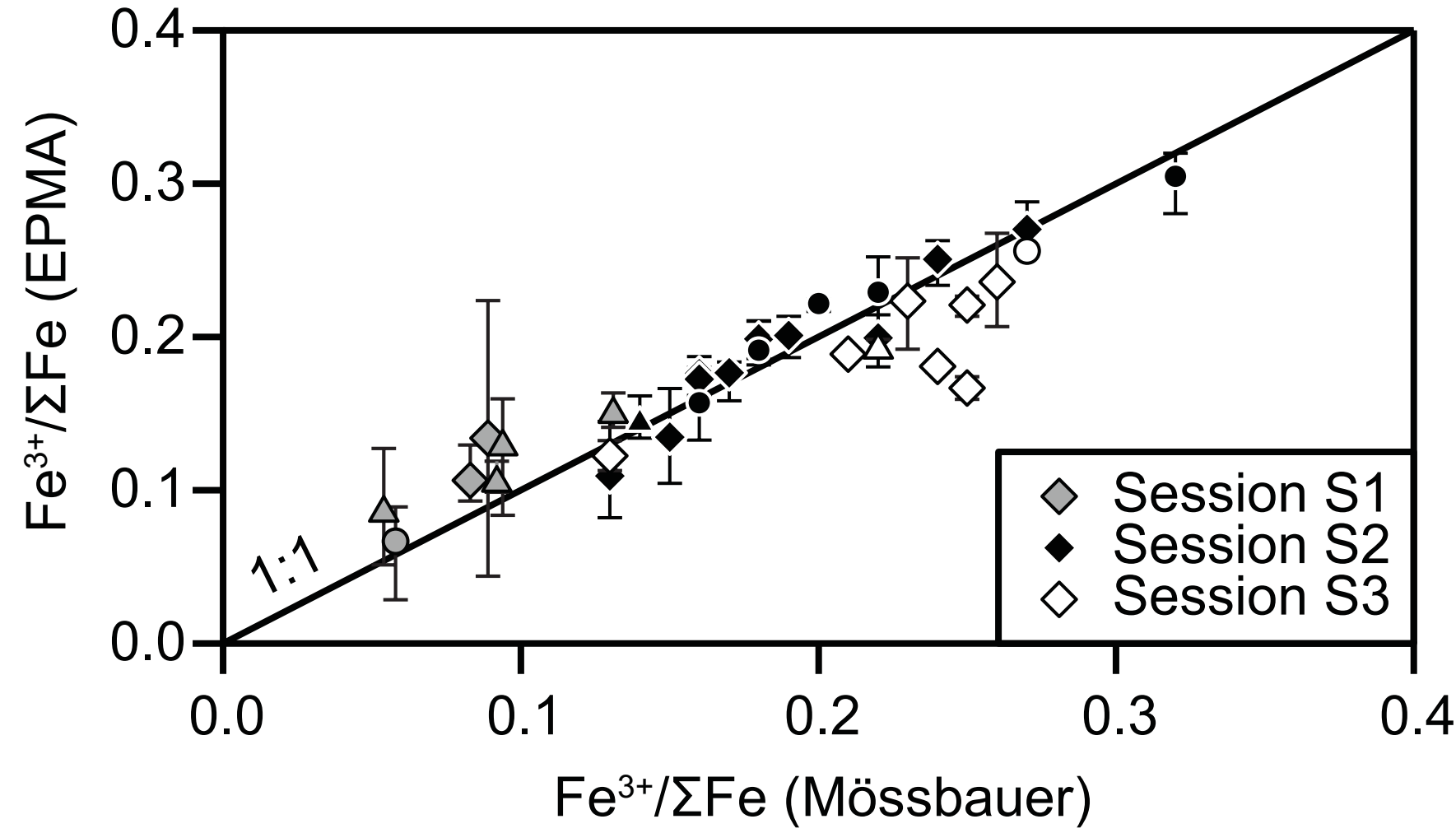
0.4
0.3
0.2
0.1
0.0
Fe3+/ΣFe (EPMA)
1:1
Session S1
Session S2
Session S3
0.0
0.1
0.2
0.3
0.4
Fe3+/ΣFe (Mössbauer)

Figure 1

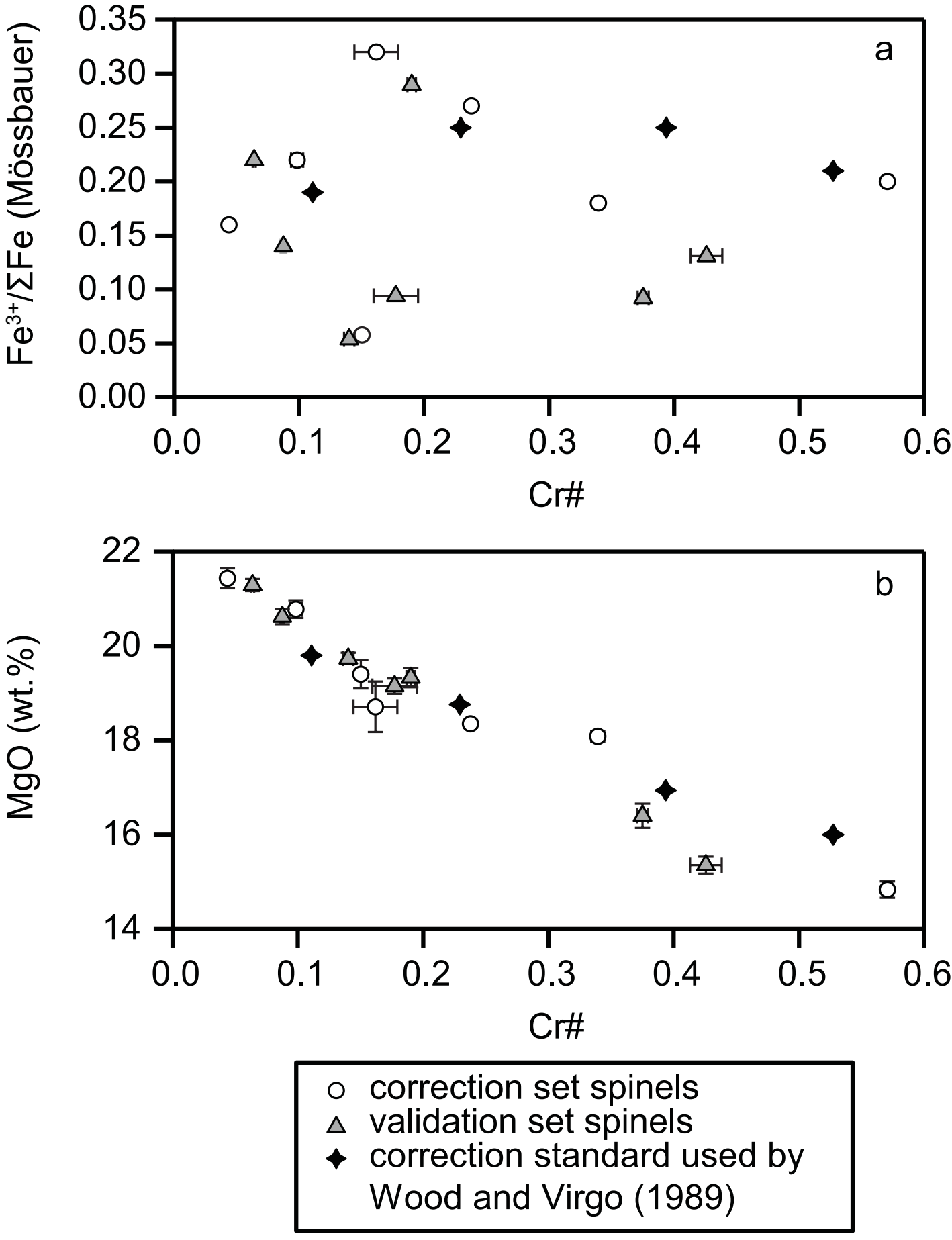
a
b
$Fe^{3+}/\Sigma Fe$ (Mössbauer)
MgO (wt.%)
Cr#
Cr#
0.35
0.30
0.25
0.20
0.15
0.10
0.05
0.00
22
20
18
16
14
0.0
0.1
0.2
0.3
0.4
0.5
0.6
correction set spinels
validation set spinels
correction standard used by Wood and Virgo (1989)

Figure 2

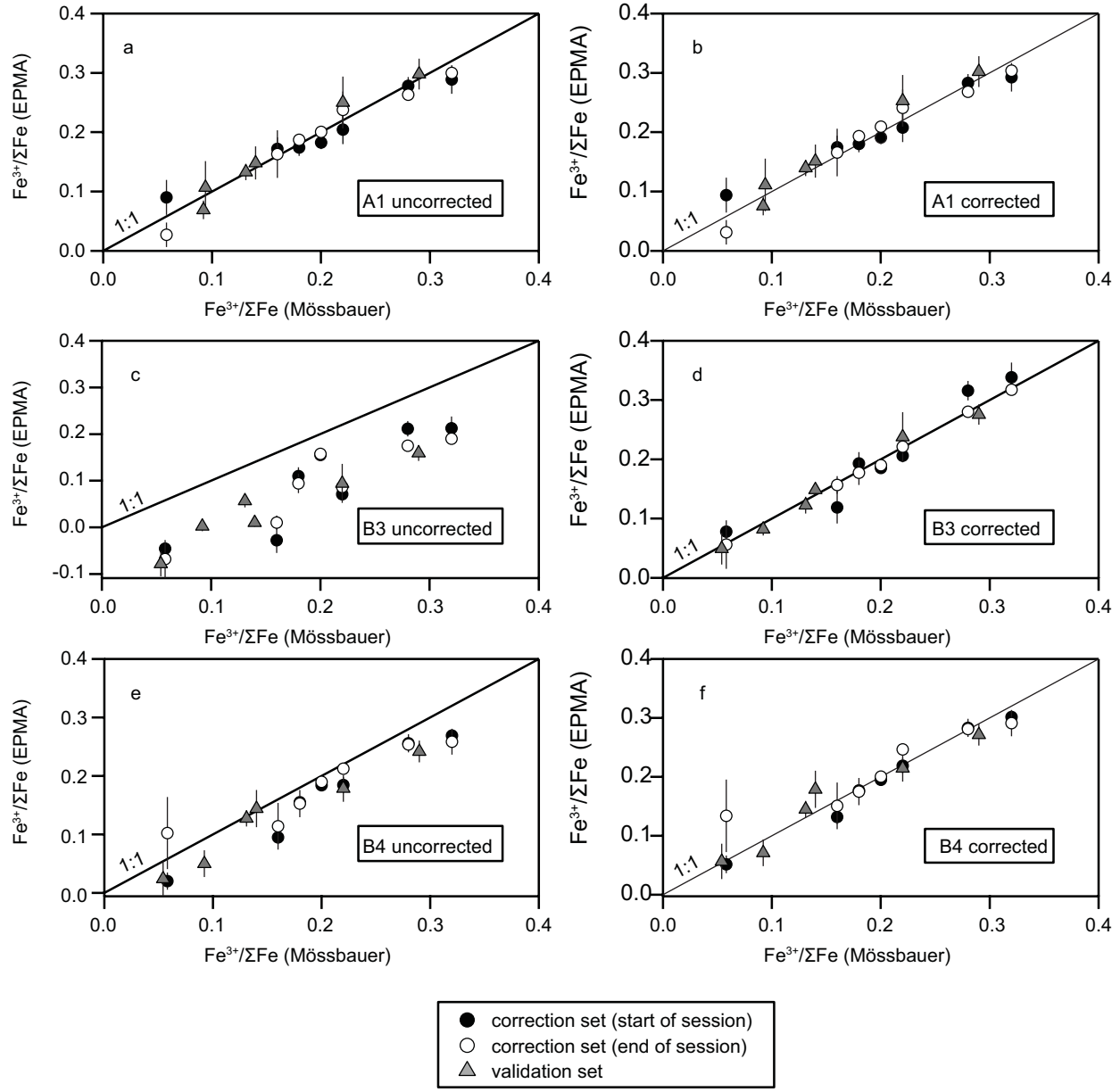
a
A1 uncorrected
b
A1 corrected
c
B3 uncorrected
d
B3 corrected
e
B4 uncorrected
f
B4 corrected
1:1
Fe3+/ΣFe (EPMA)
Fe3+/ΣFe (Mössbauer)
correction set (start of session)
correction set (end of session)
validation set

Figure 3

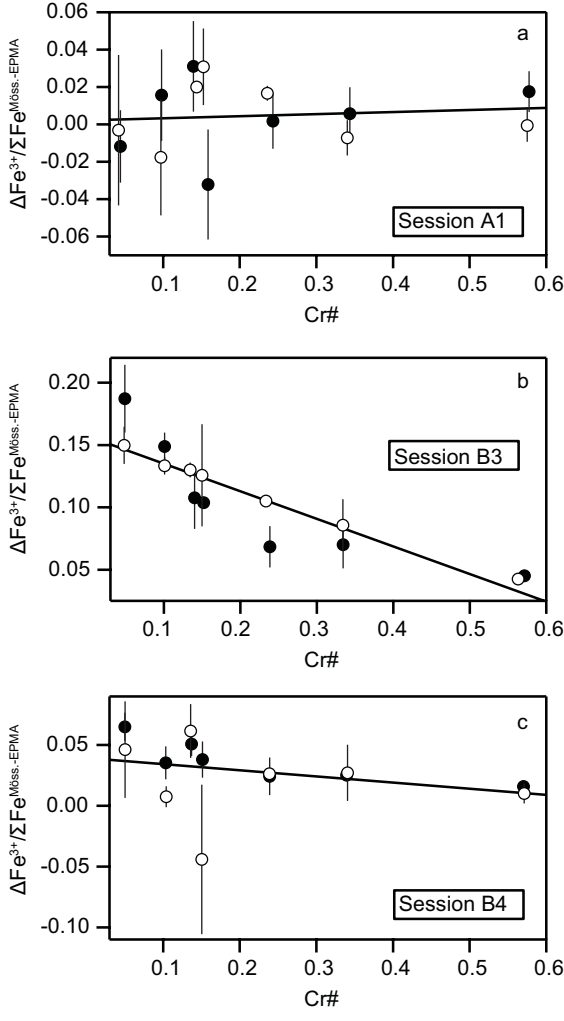
a
Session A1
$\Delta Fe^{3+}/\Sigma Fe^{Möss.-EPMA}$
Cr#
b
Session B3
$\Delta Fe^{3+}/\Sigma Fe^{Möss.-EPMA}$
Cr#
c
Session B4
$\Delta Fe^{3+}/\Sigma Fe^{Möss.-EPMA}$
Cr#

Figure 4

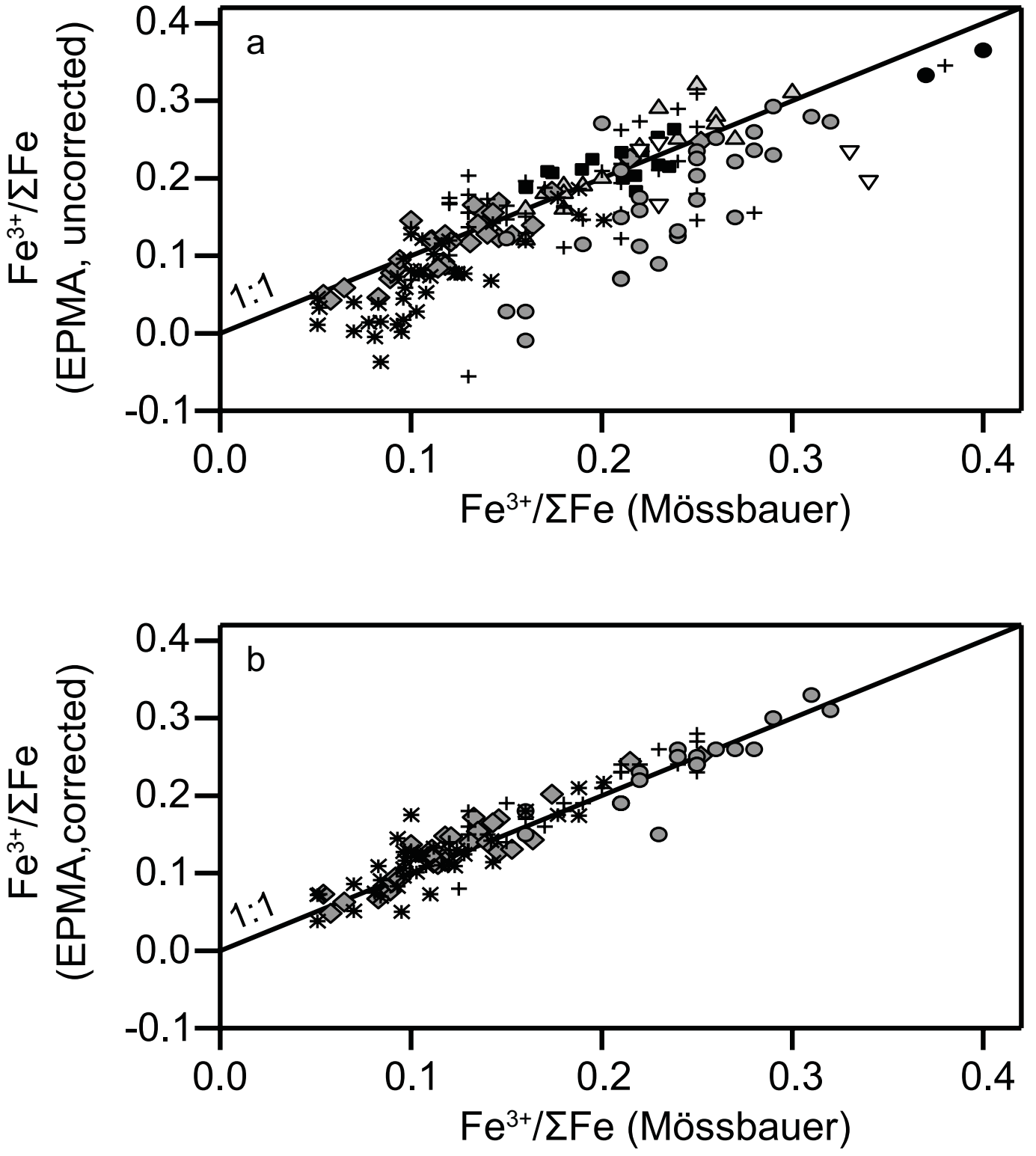

▽ Dyar et al. (1989)
△ Canil et al. (1990)
● McGuire et al. (1989)
+ Ionov and Wood (1992)
○ Wood and Virgo (1989)
✳ Woodland et al. (1992)
◇ Bryndzia and Wood (1990)
▪ Nasir (1996)

Figure 5

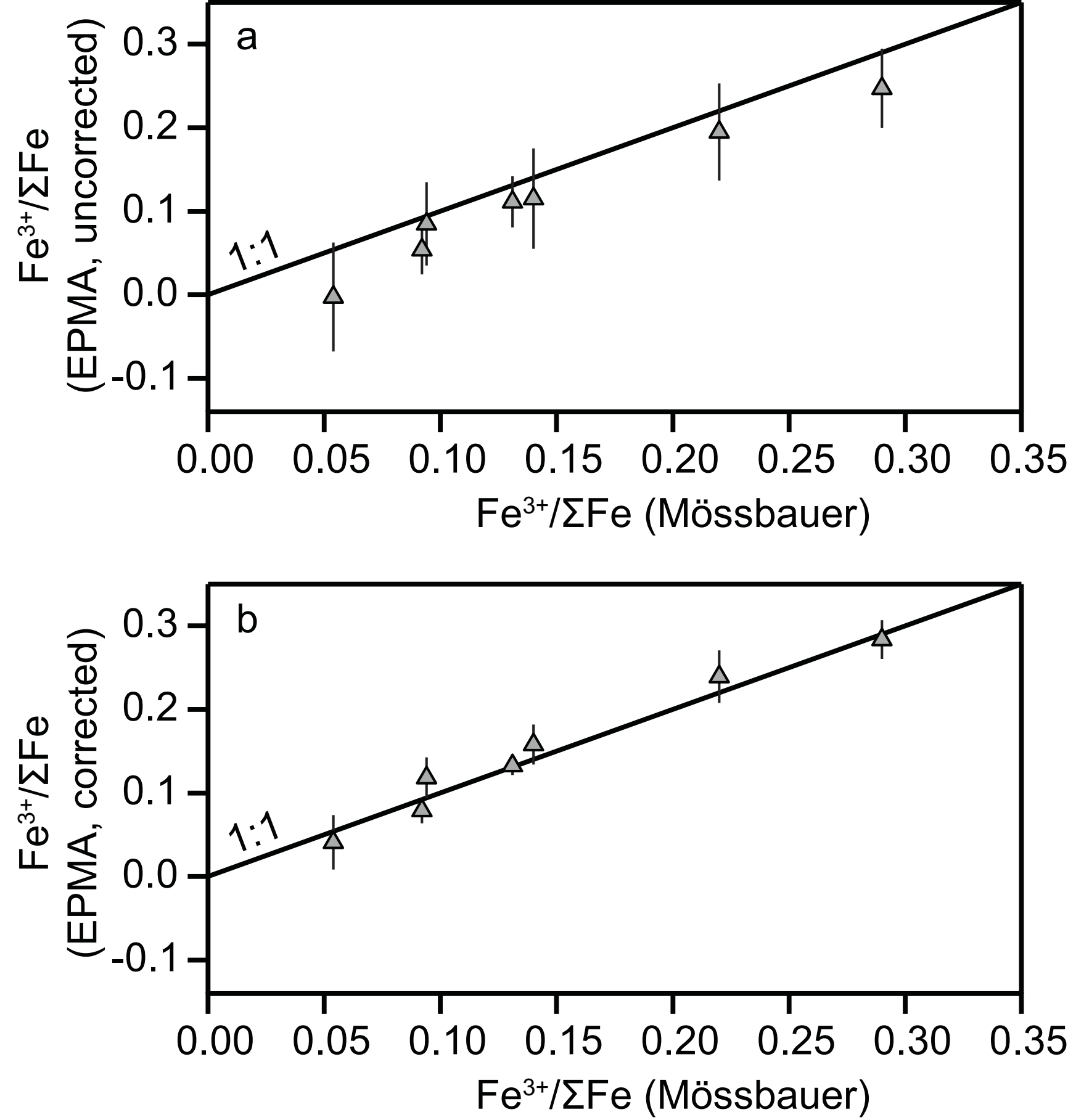
a
b
1:1
1:1
0.3
0.2
0.1
0.0
-0.1
0.00
0.05
0.10
0.15
0.20
0.25
0.30
0.35
Fe3+/ΣFe (EPMA, uncorrected)
Fe3+/ΣFe (EPMA, corrected)
Fe3+/ΣFe (Mössbauer)
Fe3+/ΣFe (Mössbauer)

Figure 6

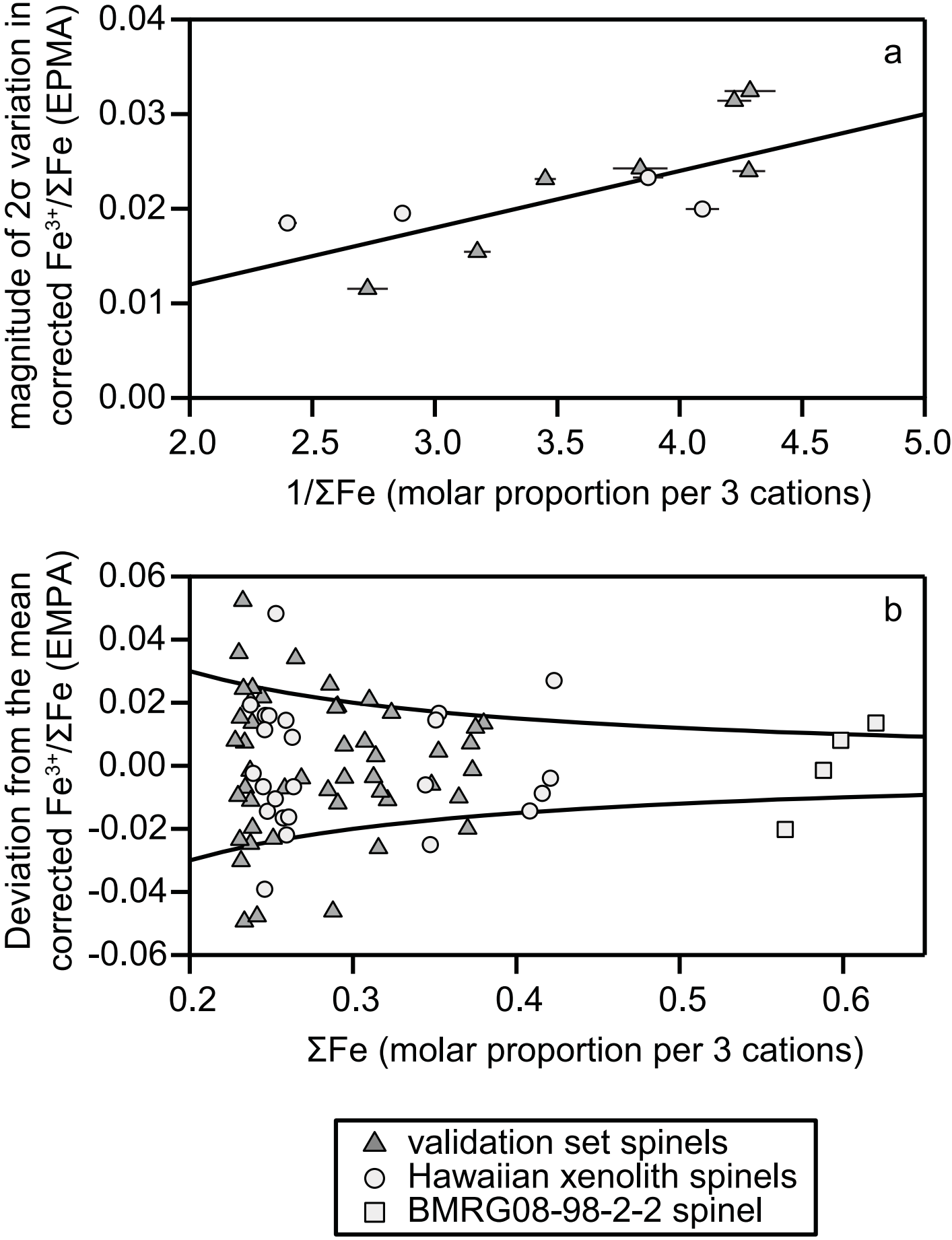
magnitude of 2σ variation in corrected Fe3+/ΣFe (EPMA)
0.04
0.03
0.02
0.01
0.00
a
2.0
2.5
3.0
3.5
4.0
4.5
5.0
1/ΣFe (molar proportion per 3 cations)
Deviation from the mean corrected Fe3+/ΣFe (EMPA)
0.06
0.04
0.02
0.00
-0.02
-0.04
-0.06
b
0.2
0.3
0.4
0.5
0.6
ΣFe (molar proportion per 3 cations)
validation set spinels
Hawaiian xenolith spinels
BMRG08-98-2-2 spinel

Figure 7

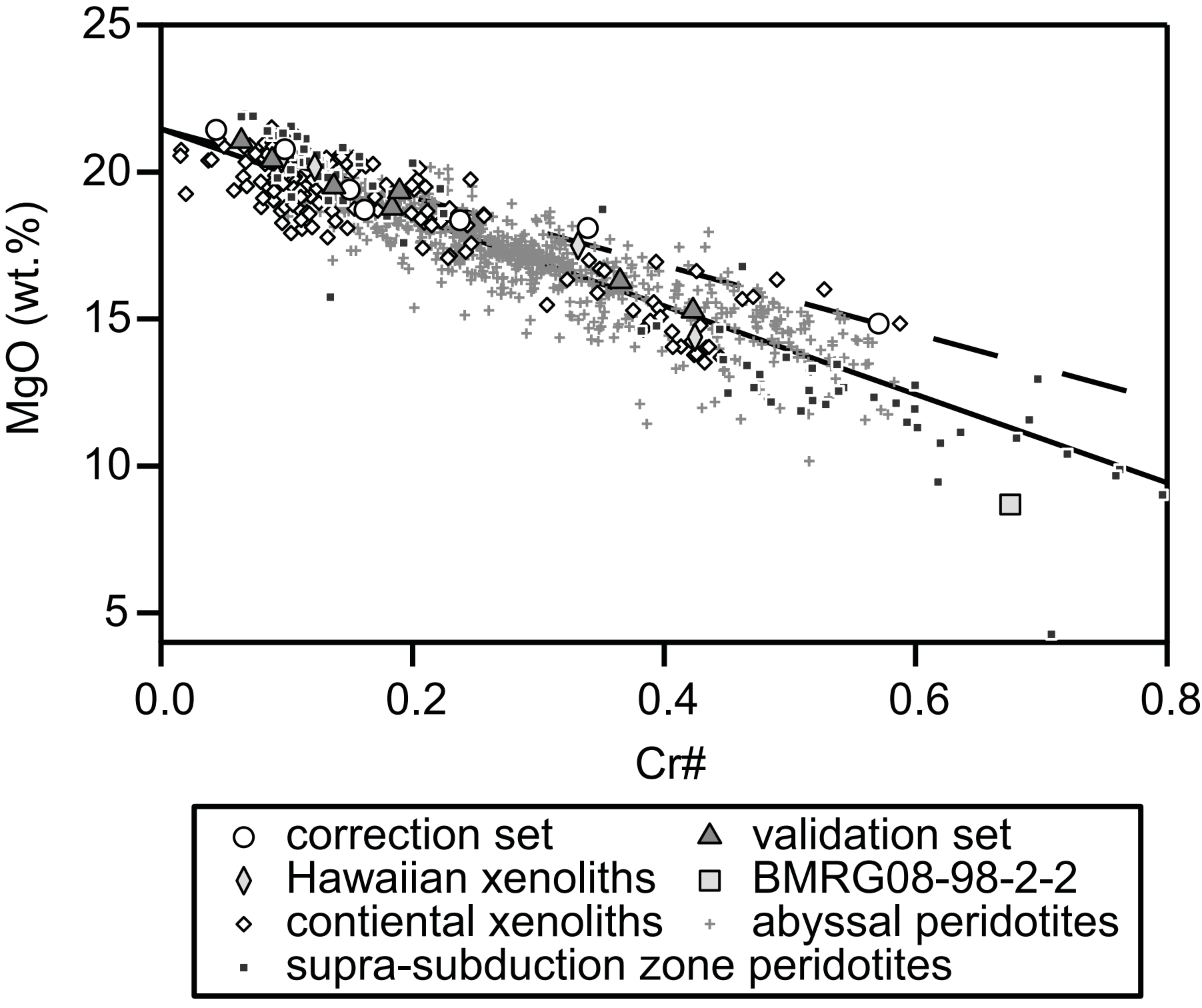
25
20
15
10
5
MgO (wt.%)
0.0
0.2
0.4
0.6
0.8
Cr#
correction set
validation set
Hawaiian xenoliths
BMRG08-98-2-2
contiental xenoliths
abyssal peridotites
supra-subduction zone peridotites

Figure 8

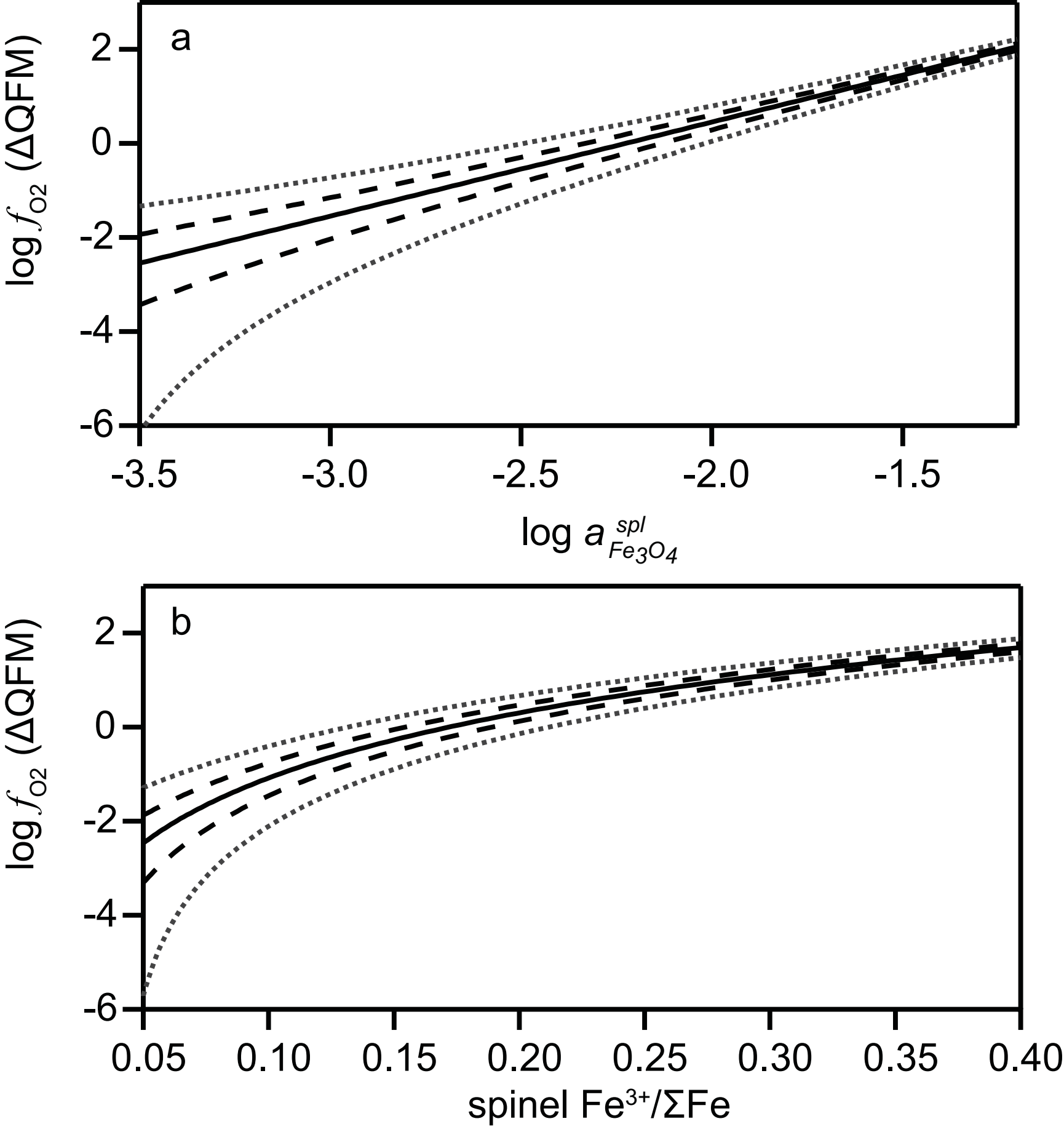
a
2
0
-2
-4
-6
log f_{O2} (ΔQFM)
-3.5
-3.0
-2.5
-2.0
-1.5
log $a^{spl}_{Fe_3O_4}$
b
2
0
-2
-4
-6
log f_{O2} (ΔQFM)
0.05
0.10
0.15
0.20
0.25
0.30
0.35
0.40
spinel $Fe^{3+}/\Sigma Fe$

Figure 9

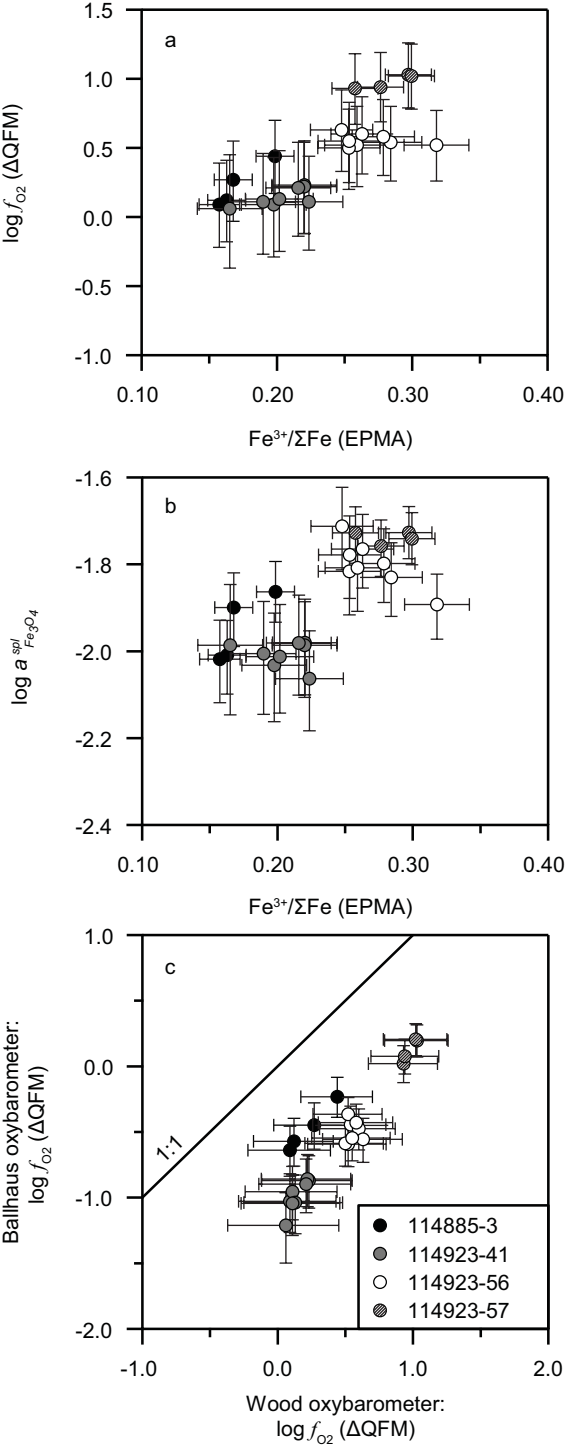
a
log f_{O2} (ΔQFM)
1.5
1.0
0.5
0.0
-0.5
-1.0
0.10
0.20
0.30
0.40
Fe3+/ΣFe (EPMA)
b
log $a^{spl}_{Fe_3O_4}$
-1.6
-1.8
-2.0
-2.2
-2.4
0.10
0.20
0.30
0.40
Fe3+/ΣFe (EPMA)
c
Ballhaus oxybarometer:
log f_{O2} (ΔQFM)
1:1
1.0
0.0
-1.0
-2.0
-1.0
0.0
1.0
2.0
Wood oxybarometer:
log f_{O2} (ΔQFM)
114885-3
114923-41
114923-56
114923-57

Figure 10